Self-consistent micromechanical approach for damage accommodation in rock-like polycrystalline materials

Journal Title
XX(X):2–37

DOI: 10.1177/ToBeAssigned
www.sagepub.com/
SAGE

Amade Pouya[1] and Cheng Zhu[2,3] and Chloé Arson[3]

Prepared using sagej.cls

Abstract

In quasi-brittle polycrystalline materials, damage by cracking or cleavage dominates plastic and viscous deformation. This paper proposes a micromechanical model for rock-like materials, incorporating the elastic-damage accommodation of the material matrix, and presents an original method to solve the system of implicit equations involved in the formulation. A self-consistent micromechanical approach is used to predict the anisotropic behavior of a polycrystal in which grain inclusions undergo intragranular damage. Crack propagation along planes of weakness with various orientation distributions at the mineral scale is modeled by a softening damage law and results in mechanical anisotropy at the macroscopic scale. One original aspect of the formulated inclusion-matrix model is the use of an explicit expression of the Hill's tensor to account for matrix ellipsoidal anisotropy. To illustrate the model capabilities, a uniaxial compression test was simulated for a variety of polycrystals made of two types of mineral inclusions with each containing only one plane of weakness. Damage always occurred in only one mineral type: the damaging mineral was that with a smaller shear modulus (respectively higher bulk modulus) when bulk modulus (respectively shear modulus) was the same. For two minerals with the same shear moduli but different bulk moduli, the maximum damage in the polycrystal under a given load was obtained at equal mineral fractions. However, for two minerals with different shear moduli, the macroscopic damage was not always maximum when the volume fraction of two minerals was the same. When the weakness planes' orientations in the damaging mineral laid within a narrow interval close to the loading direction, the macroscopic damage behavior was more brittle than when the orientations were distributed over a wider interval. Parametric studies show that upon proper calibration, the proposed model can be extended to understand and predict the micro-macro behavior of different types of quasi-brittle materials.

Keywords

polycrystal, ellipsoidal anisotropy, damage, micromechanics, self-consistent method, numerical simulation

[1]Université Paris-Est, Laboratoire Navier (UMR 8205), CNRS, Ecole des Ponts ParisTech, IFSTTAR, F-77455 Marne-la-Vallée, France
[2]Department of Civil and Environmental Engineering, Rowan University, Glassboro, NJ, USA
[3]School of Civil and Environmental Engineering, Georgia Institute of Technology, Atlanta, GA, USA

Corresponding author:
Cheng Zhu, Department of Civil and Environmental Engineering, Rowan University, Glassboro, NJ 08028, USA
Email: zhuc@rowan.edu

Prepared using sagej.cls *[Version: 2016/06/24 v1.10]*

Introduction

Great progress has been made in micromechanical modeling of heterogeneous materials since the pioneering work of Eshelby (1957) on the deformation of an ellipsoidal inclusion (also called grain) embedded in an infinite and linear elastic matrix. From there, Kröner (1961) was the first to extend the self-consistent method of Hershey (1954) to the elastic-plastic behavior of polycrystalline materials. However, these first developments were based on the assumption that the interaction between the material matrix and the inclusion is elastic, i.e. that the presence of the inclusion induces only a perturbation of the elastic strain of the matrix, in the vicinity of the inclusion. Many works then focused on accounting for the nonlinearity of the matrix behavior, or the so called non-linear accommodation of the matrix, in the inclusion-matrix interaction model. Hill (1965a,b) introduced two key novelties which facilitated further developments. First, the model of inclusion subjected to a free strain and then placed in the matrix was replaced by a cavity embedded in an infinite matrix, and subjected at its wall to surface traction and displacements. Hill's stiffness tensor was thus introduced for the cavity. Second, Hill formulated the interaction model with an incremental method instead of the original secant method, which is more suitable for nonlinear behaviors. Based on Hill's contributions, complemented by averaging theorems, many developments were made on the self-consistent method (Willis, 1977; Cleary et al., 1980; Ju, 1991; Nemat-Nasser, 2004; Nemat-Nasser and Hori, 2013; Zeng et al., 2015). It also became possible to account for plastic accommodation, as presented in a series of works starting by the one of Berveiller and Zaoui (1978) and going to more recent works by Molinari et al. (1997). The elastic-plastic model formulated by Kröner (1961) was extended to viscous behaviors by Weng (1982). However, the self consistency of Weng's model was debated by many authors such as Molinari et al. (1987) and Rougier et al. (1994). Different approaches were proposed, by Masson and Zaoui (1999), Pouya and Zaoui (1999), and Masson et al. (2000), to address the key question of how the viscous accommodation can be taken into account, in particular the exhaustive work of Mercier and Molinari (2009).

In quasi-brittle polycrystalline materials like crystalline rocks, for which granite and gneiss are common examples, damage by cracking or by cleavage on some crystallographic weakness planes dominates plastic and viscous deformation (Ju, 1996; Feng and Yu, 2010; Zeng et al., 2014; Wang et al., 2015; Zhu and Shao, 2015; Zhu et al., 2016). Modeling micromechanical damage can be done either by considering microscopic cracks explicitly in the formulation, or, in continuation of the inclusion model proposed by Eshelby in plasticity, by introducing damage in the microscopic constitutive model. Micromechanical models considering cracks were first proposed by Budiansky and O'connell (1976) and then developed by Kachanov (1980, 1992). The nonlinear behavior and load induced anisotropy due to crack closure and frictional contact were investigated based on a self-consistent

homogenization method (Horii and Nemat-Nasser, 1983; Zhu et al., 2008; Qi et al., 2016). The self-consistent approach was also used by Sumarac and Krajcinovic (1987) for investigating damage by micro-cracking. These theoretical approaches focused on the determination of the effective moduli of the solids containing a given population of cracks and not on the modeling of the dynamic damage process by crack growth. By contrast, Horii and Nemat-Nasser (1985) explained how mechanisms of crack growth at the micro-scale can determine the macroscopic failure mode for brittle materials. Rather than representing micro-crack growth explicitly, Chaboche et al. (2001) and Boudifa et al. (2009) recently extended micromechanical elastic-plastic models to damage mechanics to investigate damage processes in composite or polycrystalline materials. However, even when a self-consistent approach was used, the effect of the damage accommodation of the matrix on the inclusion-matrix interaction was not theoretically investigated. In a recent paper (Pouya et al., 2016), we presented a micromechanical approach to predict damage and viscous deformation in polycrystalline salt rock, which explained the micromechanical coupling between damage and viscous deformation, but ignored damage accommodation. The goal of the present paper is to address the theoretical and numerical challenges raised by micromechanical modeling of damage accommodation in quasi-brittle heterogeneous materials. As an example to guide discussions, a composite aggregate constituted of two types of mineral inclusions is considered. Crystalline minerals are assumed to have a plane of weakness, along which microcracks can propagate. The plane of weakness is not necessarily passing through the grain, and could actually represent a plane of weakness passing along the boundary of nonsphearical grains. A local unidirectional damage model is used to calculate the corresponding stiffness degradation at the mineral scale.

As shown by Horii and Nemat-Nasser (1983), even in a material containing a random (isotropic) distribution of cracks, a load-induced anisotropy can result from the nonlinear behavior of cracks. Cracking under mechanical loading also leads most of the time to anisotropic distributions of crack orientations, thus to anisotropic properties for the matrix (Abdul-Latif and Mounounga, 2009). In the present paper, we account for the anisotropy of the matrix in the matrix-inclusion interaction model and use an analytical expression of Hill's tensor describing the inclusion-matrix interaction, which increases the computation speed. In past homogenization work, Hill's tensor had only been exressed analytically for an isotropic matrix. Only a semi-analytical solution of the Hill tensor was available for a transverse isotropic matrix. In this study, a fully analytical expression of Hill's tensor for a particular case of transverse isotropic behavior is presented, known as ellipsoidal anisotropy (Appendix 1). Ellipsoidal anisotropy was first represented by Saint Venant (1863), who modeled amorphous anisotropic elastic solids by assuming an ellipsoidal-shape indicator surface for some elastic parameters. Although Saint Venant's work was neglected in previous literatures and cited only occasionally (Lekhnitskii, 1963), the concept of ellipsoidal anisotropy was widely adopted as a guideline for modeling elasticity in geomaterials such as soils, rocks, and concrete (Daley and Hron, 1979; Louis et al., 2004; Pouya, 2007).

As shown by Pouya (2011), the simplified data analysis and reduced number of required parameters make the concept of ellipsoidal anisotropy an attractive approach, which has diverse applications for the phenomenological and micromechanical modeling of amorphous, microcracked, or damaged materials (Halm and Dragon, 1988; Dragon et al., 2000; Sevostianov and Kachanov, 2002, 2008). The analytical solution of the ellipsoidal Hill's tensor allows the modeling of a broader range of materials than the isotropic one, and will be adopted for this reason. The behavior of the damaging grain will be represented by an ellipsoidal elasticity tensor also. In the illustration example presented below, the grain constitutive model presents transverse isotropy and depends on 3 parameters only (instead of 5 parameters in the general case). The ellipsoidal approximation is a simple and computationally efficient way to build a transversal isotropy elasticity tensor.

This paper explains a self-consistent micromechanical approach to predict the anisotropic behavior of a polycrystalline material, in which grain inclusions with different crystallographic properties undergo cracking along various planes of failure. We first describe a local damage model that is used to represent the rheological behavior of crystalline minerals (grains). Then, we explain the inclusion-matrix interaction method and provide the resulting expression of the stiffness tensor of the damaged matrix. Next, we present the iterative algorithm employed to calculate stress, strain, and damage at both macroscopic and microscopic scales. After that, we detail constitutive equations for the particular case of unidirectional damage at the grain scale. Finally, we show numerical simulation results that justify the size of the Representative Elementary Volume, illustrate the influence of the relative mechanical properties of the mineral species, and highlight the ability of the model to capture the role of the distribution of mineral orientations on damage initiation and propagation.

Grain Scale Rheological Behavior

Mechanisms of local damage at the grain scale vary significantly in different materials (Feng and Yu, 2010). In this study, grain scale or microscale refers to the scale of the inclusion embedded in a continuum matrix from the standpoint of homogenization theory, and refers to the scale of a crystal embedded in a polycrystal from the standpoint of rock physics and mechanics. In quasi-brittle polycrystalline materials, cracking by cleavage on crystallographic planes is a common mechanism, in which cracks can propagate in mode I, mode II or mixed mode along a family of weakness planes (Lee and Ju, 1991). The latter correspond to crystallographic planes that are identified as active for the given conditions of stress. In some materials, preexisting flaws can serve as stress concentrators leading to the formation of open tension microcracks (wing-cracks). The formation of wing-cracks at the tips of preexisting cracks is a common damage mechanism in quasi-brittle materials, which can take place even under global compressive stress (Horii and Nemat-Nasser, 1985; Nemat-Nasser and Obata, 1988). In this case, the

wing-cracks nucleate with some initial angle relative to the existing crack, but after a short curving stage, align themselves in the direction of the maximum principal compression and become almost straight (Paliwal and Ramesh, 2008). According to these authors, the propagation of these wing-cracks can be approximated as that of open straight cracks experiencing local tension induced by the frictional sliding of the pre-existing closed cracks. In this case, the orientation of the plane on which cracks propagate is induced by the macroscopic stress. Therefore, it is possible to use a scalar local damage criterion to account for mechanical anisotropy induced by a variety local damage mechanisms, simply by including the orientation of the weakness planes on which cracks can propagate. In this paper, we take the example of a unidirectional damage criterion that depends on the local stress $\boldsymbol{\sigma}$, the orientation $\boldsymbol{n}$ of the weakness plane on which cracks can propagate and a scalar damage variable d. The two parameters $\boldsymbol{n}$ and d are combined to form a unidirectional damage tensor $\boldsymbol{d} = d\,\boldsymbol{n} \otimes \boldsymbol{n}$. The damage criterion is thus written as $F(\boldsymbol{\sigma}, \boldsymbol{d}) \leq 0$. If there are different possible weakness planes, it will be assumed that the orientation $\boldsymbol{n}$ will be fixed by the first plane on which cracking takes place and then does not change upon damage propagation. We fixed weakness planes orientations in this model in order to have initial heterogeneity in the Representative Elementary Volume (REV), which is the minimum size required for the sample to have the same statistical mechanical response. The damage evolution law, which gives the evolution of d with deformation, depends on the physical underlying damage mechanisms. In the numerical simulation section, as an illustration example, a very simple case of the criterion F and the damage evolution law will be considered. Note that if the orientation of the plane of weakness were made dependent on the orientation of stress only, all inclusions would be initially the same because before cracking the stress state is homogeneous. Without the heterogeneity induced by the planes of weakness of fixed orientation, all micro-stresses are equal to the macro-stress, and no damage occurs. It is true that in our model, the orientation of the plane of weakness does not change after damage initiation. In future study, we could extend the present model by adding planes of weakness in damaged inclusions. At the scale of the damaged inclusion, the addition of weakness planes could thus reflect the occurrence of wing cracks, the orientation of which depends on the state of stress.

Homogenization Method

Inclusion-matrix interaction model

The inclusion-matrix interaction model is a key element in the homogenization method used in this study. Hill (1965a) introduced a general relation between small variations of stresses and strains in the inclusion $(\boldsymbol{\sigma}, \boldsymbol{\epsilon})$ and in the far-field matrix $(\overline{\boldsymbol{\sigma}}, \overline{\boldsymbol{\epsilon}})$, as follows:

$$\delta\boldsymbol{\sigma} - \delta\overline{\boldsymbol{\sigma}} = -\boldsymbol{L}^* : (\delta\boldsymbol{\epsilon} - \delta\overline{\boldsymbol{\epsilon}}) \tag{1}$$

$\boldsymbol{L}^*$ is the fourth-rank Hill's stiffness tensor, which depends on the matrix elastic properties and on the inclusion shape. For nonlinear materials, $\boldsymbol{L}^*$ is updated at each load increment. For instance, in our previous work (Pouya et al., 2016), we modeled damage in quasi-brittle salt polycrystals by introducing a macroscopic damage variable D and by updating $\boldsymbol{L}^*$ at each load increment, as follows:

$$\delta\boldsymbol{\sigma} - \delta\overline{\boldsymbol{\sigma}} = -\boldsymbol{L}^*(D) : (\delta\boldsymbol{\epsilon} - \delta\overline{\boldsymbol{\epsilon}}) \tag{2}$$

where the tensor $\boldsymbol{L}^*$ was assumed to remain constant during each load increment - an assumption that is in agreement with the concept of the interaction law (Eq. 1). However, in damaging materials, the macroscopic damage D varies in the course of the load increment. Therefore, the effect of the variation of macroscopic damage D on the variation of $\boldsymbol{L}^*$ should be taken into account. The elastic tensor of the matrix depends on the damage variable. Since the elastic tensor of the matrix is assumed to be uniform in the interaction model, the damage variable must also be assumed uniform. In this paper, we account for the variation of $\boldsymbol{L}^*(D)$ by deriving the following secant interaction model:

$$\boldsymbol{\sigma} - \overline{\boldsymbol{\sigma}} = -\boldsymbol{L}^*(D) : (\boldsymbol{\epsilon} - \overline{\boldsymbol{\epsilon}}) \tag{3}$$

Which leads to the following tangent incremental interaction law:

$$\delta\boldsymbol{\sigma} - \delta\overline{\boldsymbol{\sigma}} = -\boldsymbol{L}^*(D) : (\delta\boldsymbol{\epsilon} - \delta\overline{\boldsymbol{\epsilon}}) - \frac{\partial \boldsymbol{L}^*(D)}{\partial D} : (\boldsymbol{\epsilon} - \overline{\boldsymbol{\epsilon}})\,\delta D \tag{4}$$

where the last term translates damage accommodation, known as the irreversible alteration of the inclusion-matrix interaction stiffness tensor due to damage.

Equation (4) is an extension of equation (2), which was obtained in the case when $\boldsymbol{L}^*$ keeps constant during the load increment. In our previous work (Pouya et al., 2016), the tensor $\boldsymbol{L}^*$ was assumed isotropic. The new interaction law accounts for damage-induced anisotropy and for the damage-accommodation of the matrix during the load increment, for situations in which an analytical expression of $\boldsymbol{L}^*$ can be established. The explicit expression of the Hill's tensor $\boldsymbol{L}^*$ for an ellipsoidal type of aniostropy of the matrix, which was recently derived by the first author and presented in a work currently in preparation for publication, is given in Appendix 1. ~~In the following, we explain the anisotropic model considered for the matrix and the calculations necessary for numerical implementation.~~

Expression of the ellipsoidal anisotropic stiffness tensor of the damaged matrix

Under the assumption of ellipsoidal anisotropy, the stiffness tensor of the matrix has the following expression:

$$C_{ijkl}(\boldsymbol{D}) = \lambda D_{ij} D_{kl} + \mu \left(D_{ik} D_{jl} + D_{il} D_{jk}\right) \tag{5}$$

where λ and μ are reference (intact) values of the Lamé coefficients of the REV. This expression has been applied independently in other micromechanical investigations to characterize the effective moduli of heterogeneous media and to represent the elasticity of geomaterials (Milgrom and Shtrikman, 1992; Milton, 2002). We consider that the matrix behavior has axial symmetry about the loading axis (direction 3). Thus the damage tensor $\boldsymbol{D}$ is diagonal and $D_{11} = D_{22}$. The relation between the $\boldsymbol{D}$ components and the Young's moduli is (Pouya and Zaoui, 2006):

$$E_{\alpha\alpha}(\boldsymbol{D}) = \frac{(3\lambda + 2\mu)}{\lambda + \mu} \mu \left(D_{\alpha\alpha}\right)^2 \tag{6}$$

In order to ensure that $E_1 = E_2 = E(1 - D)$ and $E_3 = E$, we have to have: $D_{11} = D_{22} = \sqrt{1 - D}$, $D_{33} = 1$. Note that the damage tensor $\boldsymbol{D}$ is not isotropic, although its components are dependent and can be expressed as a function of unique variable D.

Micro-macro Computational Method

Micro-macro Computational Method for Strains, Stresses and Damage

At each loading step or time step t_k, known variables include $\boldsymbol{\epsilon}$, $\boldsymbol{\sigma}$, $\overline{\boldsymbol{\sigma}}$, $\overline{\boldsymbol{\epsilon}}$, D, $\boldsymbol{L}^*$ and $\frac{\partial \boldsymbol{L}^*(D)}{\partial D}$. For a given deformation increment $\delta\overline{\boldsymbol{\epsilon}}$ (respectively stress increment $\delta\overline{\boldsymbol{\sigma}}$), the goal is to calculate $\delta\boldsymbol{\epsilon}$, $\delta\boldsymbol{\sigma}$, $\delta\overline{\boldsymbol{\sigma}}$, δD (respectively $\delta\boldsymbol{\epsilon}$, $\delta\boldsymbol{\sigma}$, $\delta\overline{\boldsymbol{\epsilon}}$, δD). The numerical method requires the initial value of the stiffness of the matrix, which cannot be determined by the self-consistent method based on the initially undamaged properties of the minerals. Following the approach proposed by Hill (1952), the initial shear and bulk moduli of the composite matrix are calculated by averaging Voigt (1910) and Reuss (1929) bounds. The Voigt upper bound for the effective elastic moduli (M_V) of the matrix with two types of minerals is

$$M_V = f_1 M_1 + f_2 M_2 \tag{7}$$

The Reuss lower bound for the effective elastic moduli (M_R) of the matrix with two types of minerals is

$$\frac{1}{M_R} = \frac{f_1}{M_1} + \frac{f_2}{M_2} \tag{8}$$

where f_1 and f_2 are the volume fractions of minerals 1 and 2.

If the test is controlled in deformation ($\delta\overline{\epsilon}$), the incremental interaction law used in the computational method can be rewritten as:

$$\delta\boldsymbol{\sigma} \;=\; -\boldsymbol{L}^{*}(D) \;:\; \delta\boldsymbol{\epsilon} \;-\; \frac{\partial \boldsymbol{L}^{*}(D)}{\partial D} \;:\; (\boldsymbol{\epsilon} - \overline{\boldsymbol{\epsilon}})\,\delta D \;+\; \delta\overline{\boldsymbol{\sigma}} \;+\; \boldsymbol{L}^{*}(D) \;:\; \delta\overline{\boldsymbol{\epsilon}} \tag{9}$$

Moreover, the incremental constitutive law at the microscopic scale of the grain can be expressed as:

$$\delta\boldsymbol{\sigma} \;=\; \widetilde{\boldsymbol{C}}(\boldsymbol{d^{(n)}}) : \delta\boldsymbol{\epsilon} \;+\boldsymbol{\epsilon} : \frac{\partial \widetilde{\boldsymbol{C}}(\boldsymbol{d^{(n)}})}{\partial \boldsymbol{d^{(n)}}} : \delta\boldsymbol{d^{(n)}} \tag{10}$$

where $\boldsymbol{d^{(n)}}$ refers to the damage of the n^{th} grain.
The microscopic damage evolution law is the following:

$$\begin{aligned} &\delta\boldsymbol{d^{(n)}} \;=\; 0 \quad \text{if} \quad F(\boldsymbol{\sigma}, \boldsymbol{d^{(n)}}) < 0 \quad \text{or if} \quad F = 0 \;\text{ and }\; \tfrac{\partial F}{\partial \boldsymbol{\sigma}} : \delta\boldsymbol{\sigma} < 0 \\ &\tfrac{\partial F}{\partial \boldsymbol{\sigma}} : \delta\boldsymbol{\sigma} + \tfrac{\partial F}{\partial \boldsymbol{d^{(n)}}} : \delta\boldsymbol{d^{(n)}} = 0 \quad \text{otherwise} \end{aligned} \tag{11}$$

If $\delta\overline{\boldsymbol{\sigma}}$ and δD are given, then equations (9), (10) and (11) can be solved for the three remaining unknowns $\delta\boldsymbol{\epsilon}$, $\delta\boldsymbol{\sigma}$ and $\delta\boldsymbol{d^{(n)}}$. The values of $\delta\overline{\boldsymbol{\sigma}}^{(k)}$ and $\delta D^{(k)}$ are initialized at iteration $k = 0$. For the first iteration of the first loading increment, $\delta\overline{\boldsymbol{\sigma}}^{\boldsymbol{(0)}} = \boldsymbol{C_0} : \delta\overline{\boldsymbol{\epsilon}}$ and $\delta D^{(0)} = 0$. Then, at the first iteration of a subsequent loading increment, the values of the variables obtained at the end of the previous increment are used to set: $\delta\overline{\boldsymbol{\sigma}}^{\boldsymbol{(0)}} = \boldsymbol{C}(D) : \delta\overline{\boldsymbol{\epsilon}}$ and $\delta D^{(0)} = 0$ for an unloading path; $\delta\overline{\boldsymbol{\sigma}}^{\boldsymbol{(0)}}$ and $\delta D^{(0)}$ for a loading path. For any iteration k, equations (9), (10) and (11) are used to calculate $\delta\boldsymbol{\epsilon}^{\boldsymbol{(k)}}$, $\delta\boldsymbol{\sigma}^{\boldsymbol{(k)}}$ and $\delta\boldsymbol{d^{(n)}}^{(k)}$ from $\delta\overline{\boldsymbol{\sigma}}^{\boldsymbol{(k)}}$ and $\delta D^{(k)}$. Then the incremental macroscopic stress is updated by averaging: $\delta\overline{\boldsymbol{\sigma}}^{(k+1)} = \left\langle \delta\boldsymbol{\sigma}^{(k)} \right\rangle$. In the proposed algorithm, the updated microscopic damage in the grains and the updated macroscopic phenomenological damage variable may lead to two different values for the macroscopic damaged stiffness tensor. The convergence between the two values is checked iteratively.

First, the macroscopic damaged stiffness tensor is calculated by combining the microscopic constitutive relation: $\boldsymbol{\sigma} = \boldsymbol{C}(\boldsymbol{d^{(n)}}) : \boldsymbol{\epsilon}$ and the interaction law in equation (3):

$$\boldsymbol{\sigma} \;=\; \boldsymbol{C}(\boldsymbol{d^{(n)}}) \;:\; \Big(\boldsymbol{C}(\boldsymbol{d^{(n)}}) + \boldsymbol{L}^{*}(D)\Big)^{-1} \;:\; (\overline{\boldsymbol{\sigma}} + \boldsymbol{L}^{*}(D) : \overline{\boldsymbol{\epsilon}}) \tag{12}$$

By taking the average:

$$\overline{\boldsymbol{\sigma}} = \underbrace{\left\langle \boldsymbol{C}(\boldsymbol{d^{(n)}}) : \left(\boldsymbol{C}(\boldsymbol{d^{(n)}}) + \boldsymbol{L^*}(D)\right)^{-1} \right\rangle}_{\boldsymbol{W}} : (\overline{\boldsymbol{\sigma}} + \boldsymbol{L^*}(D) : \overline{\boldsymbol{\epsilon}}) \tag{13}$$

Replacing $\left\langle \boldsymbol{C}(\boldsymbol{d^{(n)}}) : \left(\boldsymbol{C}(\boldsymbol{d^{(n)}}) + \boldsymbol{L^*}(D)\right)^{-1} \right\rangle$ by $\boldsymbol{W}$, we have:

$$\overline{\boldsymbol{\sigma}} = (\boldsymbol{I} - \boldsymbol{W})^{-1} : \boldsymbol{W} : \boldsymbol{L^*}(D) : \overline{\boldsymbol{\epsilon}} \tag{14}$$

where $\boldsymbol{I}$ is the fourth-order identity tensor. By replacing $(\boldsymbol{I} - \boldsymbol{W})^{-1}$ as $\boldsymbol{Z}$, we have $\boldsymbol{W} = \boldsymbol{I} - \boldsymbol{Z}^{-1}$. Therefore, $(\boldsymbol{I} - \boldsymbol{W})^{-1} : \boldsymbol{W} = \boldsymbol{Z} : \left(\boldsymbol{I} - \boldsymbol{Z}^{-1}\right) = \boldsymbol{Z} - \boldsymbol{I}$. Finally:

$$\overline{\boldsymbol{\sigma}} = \underbrace{\left[(\boldsymbol{I} - \boldsymbol{W})^{-1} - \boldsymbol{I}\right]}_{\boldsymbol{C^h}} : \boldsymbol{L^*}(D) : \overline{\boldsymbol{\epsilon}} \tag{15}$$

$\boldsymbol{C^h}$ is the solution obtained by upscaling the matrix stiffness tensor from the damaged stiffness tensors of the microscopic inclusions.

In a second step, the macroscopic damaged stiffness tensor (noted: $\boldsymbol{C^d}$) is calculated from the updated value of the macroscopic damage variable: $D + \delta D$, in which $\delta D = \delta D^{(k)}$ is taken from the previous iteration. According to equation (5), we have:

$$\begin{aligned}
C^d_{1111} &= C^d_{2222} = (1 - D - \delta D)(\lambda + 2\mu) & C^d_{3333} &= \lambda + 2\mu \\
C^d_{1122} &= (1 - D - \delta D)\lambda & C^d_{1133} &= C^d_{2233} = \lambda\sqrt{1 - D - \delta D} \\
C^d_{1212} &= (1 - D - \delta D)\mu & C^d_{1313} &= C^d_{2323} = \mu\sqrt{1 - D - \delta D}
\end{aligned} \tag{16}$$

Lastly, the parameters λ, μ and $D + \delta D$ are calculated iteratively in order to minimize the distance $\|\boldsymbol{C^h} - \boldsymbol{C^d}\|$. Equation (16) shows that D is not just a scaling parameter of λ and μ, but also reflects differently the different components of $\boldsymbol{C^d}$.

The incremental interaction law in equation (9) is deduced from a simplified, approximate constitutive law of the matrix, written as $\delta\overline{\boldsymbol{\sigma}} = \boldsymbol{C}(D) : \delta\overline{\boldsymbol{\epsilon}} + \frac{\partial \boldsymbol{C}(D)}{\partial D} : \overline{\boldsymbol{\epsilon}}\,\delta D$. Note that this is a common homogenization procedure: the inclusion-matrix interaction law is constructed from an approximate, yet-unknown matrix constitutive law. According to the incremental constitutive law of the matrix, the

distance:

$$\|\delta\overline{\boldsymbol{\sigma}} - \boldsymbol{C}(D) : \delta\overline{\boldsymbol{\epsilon}} - \frac{\partial \boldsymbol{C}(D)}{\partial D} : \overline{\boldsymbol{\epsilon}}\,\delta D\| \tag{17}$$

is minimized for the converged value of δD. Taking the average of the incremental interaction law, (equation (9)) we also note that:

$$\langle\delta\boldsymbol{\sigma}\rangle = -\boldsymbol{L}^*(D) : \langle\delta\boldsymbol{\epsilon}\rangle - \frac{\partial \boldsymbol{L}^*(D)}{\partial D} : (\langle\boldsymbol{\epsilon}\rangle - \overline{\boldsymbol{\epsilon}})\,\delta D + \delta\overline{\boldsymbol{\sigma}} + \boldsymbol{L}^*(D) : \delta\overline{\boldsymbol{\epsilon}} \tag{18}$$

The condition $\langle\boldsymbol{\epsilon}\rangle = \overline{\boldsymbol{\epsilon}}$ is always satisfied. Moreover, by construction of the computational method, $\langle\delta\boldsymbol{\sigma}\rangle = \delta\overline{\boldsymbol{\sigma}}$. Therefore we have:

$$0 = \boldsymbol{L}^*(D) : (\delta\overline{\boldsymbol{\epsilon}} - \langle\delta\boldsymbol{\epsilon}\rangle) \tag{19}$$

Since $\boldsymbol{L}^*(D)$ is positive definite, we verify that $\delta\overline{\boldsymbol{\epsilon}} = \langle\delta\boldsymbol{\epsilon}\rangle$.

Example of Unidirectional Damage in Mode I at the Grain Scale

To illustrate the formulated micro-macro modeling approach, we consider a simple damage mechanism at the grain scale: the grain stiffness decreases in one direction perpendicular to a plane of weakness due to the propagation of cracks along that plane in mode I. The effect of cracking in the grain is thus represented by a uniform damage process at the grain scale. We note $\boldsymbol{n}^{(n)}$ the vector normal to the plane of weakness of the n-th grain (Figure 1). We have $\boldsymbol{n} = [sin\theta cos\phi \;\; sin\theta sin\phi \;\; cos\theta]$, in which the angles θ and ϕ are shown in Figure 1. Note that angles ψ and ϕ have no influence on the initiation and evolution

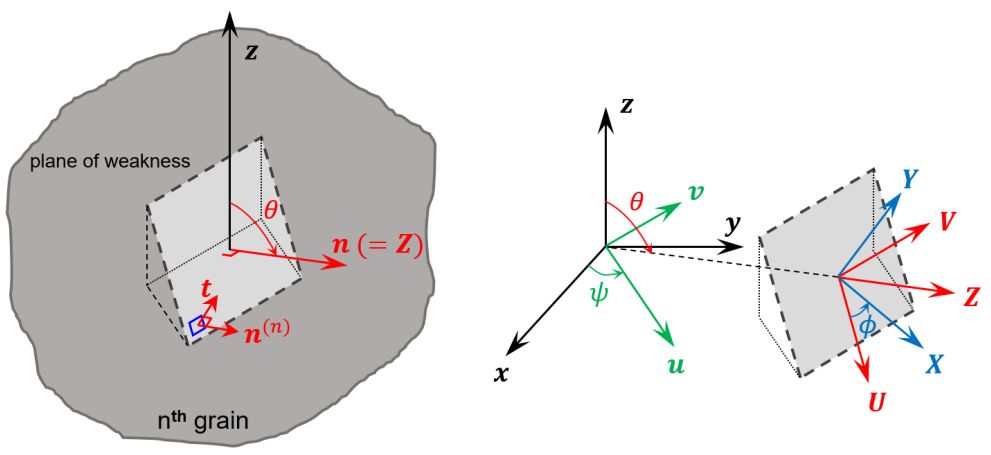

Figure 1. Local coordinate system in the plane of weakness of a grain.

of microcrack along the plane of weakness because of the axis of symmetry about the loading axis and about the direction normal to the weakness plane. Denoting $d^{(n)}$ the microscopic damage of the n^{th} grain, we have:

$$\boldsymbol{d^{(n)}} = d^{(n)}\, \boldsymbol{n^{(n)}} \otimes \boldsymbol{n^{(n)}} \tag{20}$$

Following the approach proposed by Chaboche (1992), we define the microscopic effective stress $\widetilde{\boldsymbol{\sigma}}^{(n)}$ (in the sense of Continuum Damage Mechanics) as:

$$\widetilde{\boldsymbol{\sigma}}^{(n)} = \boldsymbol{M}(\boldsymbol{d^{(n)}}) : \boldsymbol{\sigma^{(n)}} \tag{21}$$

where $\boldsymbol{M}(\boldsymbol{d^{(n)}})$ is a fourth-order operator, called "damage operator" in the following. According to the Principle of Equivalent Elastic Energy, the damaged stiffness tensor is expressed as:

$$\widetilde{\boldsymbol{C}}(\boldsymbol{d^{(n)}}) = \boldsymbol{M}^{-1}(\boldsymbol{d^{(n)}}) : \boldsymbol{C_0} : \boldsymbol{M}^{-T}(\boldsymbol{d^{(n)}}) \tag{22}$$

where $\boldsymbol{C_0}$ is the stiffness tensor of the undamaged grain, assumed to be linear elastic. Hence the damaged stiffness tensor depends on three parameters: the two Lamé coefficients (in $\boldsymbol{C_0}$) and the damage variable $\boldsymbol{d^{(n)}}$. The expression of $\widetilde{\boldsymbol{C}}$ is not known though. The assumption of ellipsoidal anisotropy allows constraining the expression of $\widetilde{\boldsymbol{C}}$, as shown in Eq. 67 presented in Appendix 2.

At the grain scale, for mode I cracking, damage initiates when the maximum microscopic principal stress exceeds the tensile strength of the grain (σ_T) and that after damage initiation, the direction of damage is fixed and the microscopic stress-strain relationship follows a law similar to plasticity with linear softening. The damage criterion takes the following expression:

$$F(\boldsymbol{\sigma}, \boldsymbol{d^{(n)}}) = \left(\boldsymbol{n^{(n)}} \otimes \boldsymbol{n^{(n)}}\right) : \boldsymbol{\sigma} - \sigma_T\, g(\boldsymbol{d^{(n)}}) \tag{23}$$

where $\boldsymbol{n^{(n)}}$ is the direction in which the maximum principal stress exceeds the tensile strength for the first time. The resistance of the damaged grain to deformation is assumed to vary linearly with deformation. We choose $g(\boldsymbol{d^{(n)}})$ in order to capture this softening behavior. The microstress in direction $\boldsymbol{n^{(n)}}$ is expressed as:

$$\left(\boldsymbol{n^{(n)}} \otimes \boldsymbol{n^{(n)}}\right) : \boldsymbol{\sigma} = \left(\boldsymbol{n^{(n)}} \otimes \boldsymbol{n^{(n)}}\right) : \widetilde{\boldsymbol{C}}(\boldsymbol{d^{(n)}}) : \boldsymbol{\epsilon} \tag{24}$$

Moreover, the softening law can be written as:

$$\left(\boldsymbol{n^{(n)}} \otimes \boldsymbol{n^{(n)}}\right) : \boldsymbol{\sigma} = \sigma_T\, g(\boldsymbol{d^{(n)}}) = \left(1 - \frac{\epsilon_{nn} - \epsilon_0}{\epsilon_f - \epsilon_0}\right) \sigma_T \tag{25}$$

where ϵ_{nn} is the microscopic strain normal to direction $\boldsymbol{n^{(n)}}$, ϵ_0 is the normal strain at which damage initiates and ϵ_f is the normal strain at which the normal stress vanishes (Figure 2).

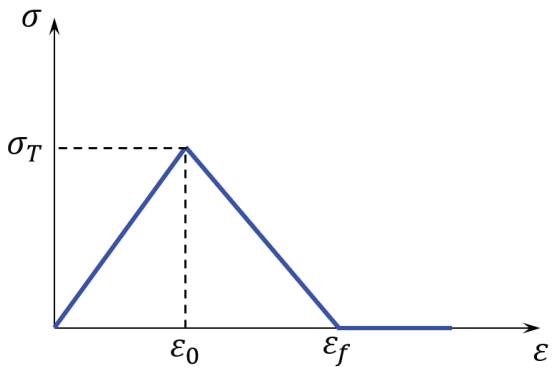

Figure 2. Damage criterion at the grain scale.

From equation (67) in Appendix 2, we have:

$$\boldsymbol{\sigma} \;=\; \lambda_0\,\epsilon_v\,\boldsymbol{\delta} \;+ 2\mu_0\,\boldsymbol{\epsilon} \;+ \left(d^{(n)}\right)^2\left(\lambda_0+2\mu_0\right)\epsilon_{nn}\boldsymbol{n^{(n)}}\otimes\boldsymbol{n^{(n)}} \;- d^{(n)}\lambda_0\left[\epsilon_{nn}\boldsymbol{\delta} \;+\epsilon_v\boldsymbol{n^{(n)}}\otimes\boldsymbol{n^{(n)}}\right]$$
$$-2\,d^{(n)}\mu_0\left[\left(\boldsymbol{\epsilon}\cdot\boldsymbol{n^{(n)}}\right)\otimes\boldsymbol{n^{(n)}} \;+\boldsymbol{n^{(n)}}\otimes\left(\boldsymbol{\epsilon}\cdot\boldsymbol{n^{(n)}}\right)\right] \tag{26}$$

After some computations, a projection on $\boldsymbol{n^{(n)}}\otimes\boldsymbol{n^{(n)}}$ provides:

$$\sigma_T\,g(\boldsymbol{d^{(n)}}) \;=\; (1-d^{(n)})\;\left[\lambda_0\epsilon_v \;+(-d^{(n)}\lambda_0+2(1-d^{(n)})\mu_0)\epsilon_{nn}\right] \tag{27}$$

Let us note $\boldsymbol{t}$ a direction perpendicular to $\boldsymbol{n^{(n)}}$ (Figure 1). If the grain is subjected to a uniaxial stress condition, then $\boldsymbol{t}\cdot\boldsymbol{\sigma}\cdot\boldsymbol{t}\;=0$. From equation (26), this condition can be expressed as:

$$0 \;=\; \lambda_0\epsilon_v \;+2\mu_0\epsilon_{tt} \;- d^{(n)}\lambda_0\epsilon_{nn} \tag{28}$$

where ϵ_{tt} is the microscopic strain in a direction $\boldsymbol{t}$ in the weakness plane. In uniaxial stress conditions, we have: $\epsilon_v=\epsilon_{nn}+2\epsilon_{tt}$, which leads to:

$$\epsilon_{tt} \;=\; -(1-d^{(n)})\frac{\lambda_0}{2(\lambda_0+\mu_0)}\epsilon_{nn}, \qquad \epsilon_v \;=\; \frac{\lambda_0 d^{(n)}+\mu_0}{\lambda_0+\mu_0}\epsilon_{nn} \tag{29}$$

Now combining equations (27) and (29), we find:

$$\sigma_T\, g(\boldsymbol{d^{(n)}}) \;=\; \left(1-d^{(n)}\right)^2 \frac{3\lambda_0+2\mu_0}{\lambda_0+\mu_0}\mu_0\epsilon_{nn} \;=\; \left(1-d^{(n)}\right)^2 E_0\,\epsilon_{nn} \tag{30}$$

where E_0 the Young's modulus that corresponds to the Lamé coefficients λ_0 and μ_0. Noticing that $\sigma_T = E_0\epsilon_0$, and using the softening law in equation (25), we get:

$$g(\boldsymbol{d^{(n)}}) \;=\; \frac{(1+\eta)\left(1-d^{(n)}\right)^2}{1+\eta\left(1-d^{(n)}\right)^2}, \qquad \eta = \frac{\epsilon_f-\epsilon_0}{\epsilon_0} \tag{31}$$

If $\eta = 0$, the material is elastic-brittle, i.e. the resistance to deformation falls to zero as soon as the damage criterion is reached. If $\eta \to \infty$, $g(\boldsymbol{d^{(n)}}) \to 1$, i.e. the material is perfectly plastic.
From the calculations above, we can express the damage criterion (equation (23)) in terms of deformation, as follows:

$$F(\boldsymbol{\epsilon}, \boldsymbol{d^{(n)}}) \;=\; \left(1-d^{(n)}\right) \times \left(\lambda_0\epsilon_v \;+\; \left[-d^{(n)}\lambda_0 + 2(1-d^{(n)})\mu_0\right]\epsilon_{nn}\right) \;-\; \sigma_T\, g(\boldsymbol{d^{(n)}}) \tag{32}$$

Numerical Simulations

In order to understand the influence of the elastic properties of individual grains, the orientations of the planes of weakness and the mineral fraction, we conduct a parametric study on a polycrystalline material that contains two mineral constituents. Each mineral is represented by a finite number of grains with different weakness plane orientations which follow a uniform distribution. This model allows simulations of complex stress paths such as loading and unloading cycles and different boundary conditions. Here, we only present the results of uniaxial loading simulations in order to focus on the fundamental mechanism of grain-matrix interaction.

Calibration of the Model Parameters

We calibrate the model parameters against published experimental data obtained from a uniaxial compression test performed on granite (Halm and Dragon, 2002). Here we consider that granite as a mixture of two types of minerals, quartz and feldspar. Each mineral is represented by 200 grains, i.e. each mineral species has the same volume fraction. The next section presents a sensitivity analysis of the number of grains. The orientations of the planes of weakness (θ in Figure 1) are uniformly distributed within the range 0 to $\pi/2$. We choose $\sigma_T = 6$ MPa for both minerals, which corresponds to the tensile strength of granite (Perras and Diederichs, 2014). We take 0.7 for the brittleness indicator η, in order to

capture the quasi-brittle behavior of the minerals. The calibrated values obtained for the shear and bulk moduli of the two minerals are reported in Table 1. Calibrated elastic properties fall within the typical range of values for quartz (Heyliger et al., 2003) and feldspar (Brown et al., 2016). As expected, quartz has a larger shear modulus than feldspar and and is relatively harder.

Table 1. Calibrated shear modulus and bulk modulus for quartz and feldspar in a granite sample.

Mineral Type	quartz		feldspar	
Elastic Properties	μ_1 (MPa)	K_1 (MPa)	μ_2 (MPa)	K_2 (MPa)
Calibrated Value	4.07×10^4	6.17×10^4	2.67×10^4	6.14×10^4

The simulated stress-strain response matches well the experimental data. In Figure 3(a), solid lines represent the purely elastic response and dashed lines indicate an extension of the elastic behavior. It can be seen that the stress/strain curve deviates slightly from the elastic response during the experiment in the lateral direction. This observation suggests that a small amount of damage was produced in the material under uniaxial compression. Damage initiates when the uniaxial stress reaches about 38 MPa, as indicated by the evolution of macroscopic damage (Figure 3(b)), consistent with experimental observations in Figure 3(a). After initiation, damage propagation is nonlinear: the positive damage rate gradually slows down as the applied stress becomes larger. We note that the value of macroscopic damage is small, which explains the quasi-linear stress-strain relation obtained at the matrix scale.

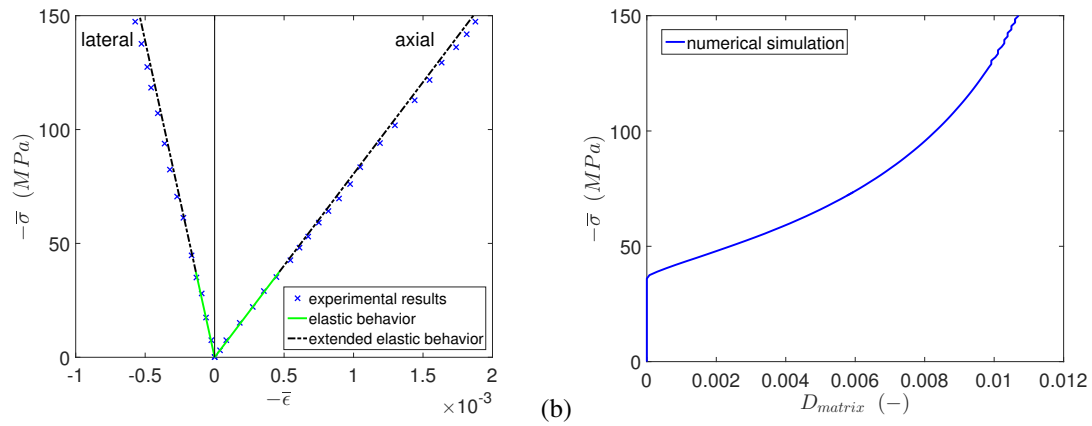

(a) (b)

Figure 3. Measured and simulated uniaxial compression curves for granite: (a) Experimental stress-strain relation (Halm and Dragon, 2002); (b) Simulated macroscopic damage evolution.

Model Sensitivity to the Number of Grains

In order to eliminate the influence of the sample size on the computational results, we first carry out a sensitivity analysis on the total number of grains in the polycrystalline material, which is often overlooked in polycrystal simulations (Wu et al., 1996; Buchheit et al., 2005). This is equivalent to examining the mesh size dependence in a finite element method-based approach. For simplicity, we round up the calibrated values of the mineral elastic parameters to the nearest integers in the following simulations (Table 2). We study the influence of the number of grains when both minerals have the same shear modulus but different bulk moduli (scenario 1) and when both minerals have the same bulk modulus but different shear moduli (scenario 2). The number of grains varies between 5 to 400 but is the same for both mineral types. Since the sensitivity analysis could refer to any composite material, and not only a granite made of quartz and feldspar, we denote the mineral types A and B. For both types of minerals, the orientations of the planes of weakness are assumed to be uniformly distributed in the domain of $[0,\ \pi/2]$.

Table 2. Input parameters for mineral A and mineral B in the two scenarios used for the sensitivity analysis on the number of grains.

Mineral Type	Mineral A			Mineral B		
Elastic Properties	μ_A (MPa)	K_A (MPa)	N_A	μ_B (MPa)	K_B (MPa)	N_B
Scenario 1	4×10^4	6×10^4	$5 \sim 400$	4×10^4	18×10^4	$= N_A$
Scenario 2	1×10^4	6×10^4	$5 \sim 400$	4×10^4	6×10^4	$= N_A$

Figure 4 shows that in both scenarios, the variations of the macroscopic damage in the matrix is sensitive to the total number of grains when $N_A = N_B$ is less than 200. Above that threshold, the ultimate matrix damage stabilizes and tends to an asymptotic value and becomes independent of the total number of grains. This simulations validate the calibration presented above with 200 grains for each mineral species. Hence, we assign 200 grains to each mineral type to ensure statistical representation of the orientations of the planes of weakness at minimal computational cost.

Influence of Minerals' Shear Modulus

We compare two composites made of two mineral constituents of equal bulk modulus but distinct shear moduli, both represented by 200 grains with weakness planes, the orientation of which are uniformly distributed in the $[0,\ \pi/2]$ interval. We study two cases S1 and S2, described in Table 3.

Results are shown in Figure 5. Macroscopic damage accumulates faster and initiates under lower stress in case S2 than in case S1, because the overall shear modulus of the matrix is lower in case S2 than in case S1 (Figure 5(a)). The rate of damage propagation decreases as damage accumulates, as the number of damaged grains reaches an asymptotic value when the stress level increases (Figure 5(b)).

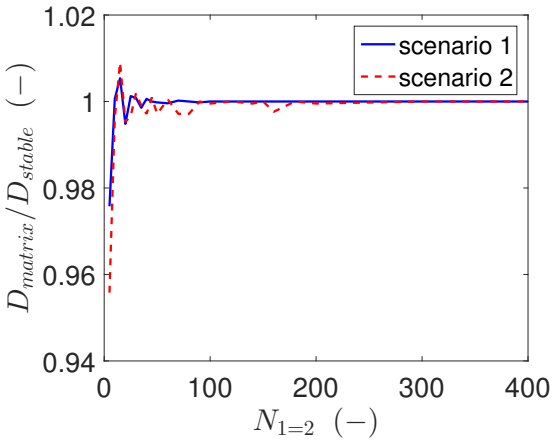

Figure 4. Dependence of matrix damage on the number of grains used to represent each mineral type ($N_1 = N_2$).

Table 3. Elastic properties of the two minerals used to study the influence of the shear modulus.

Mineral Type	Mineral A		Mineral B	
Elastic Properties	μ_A (MPa)	K_A (MPa)	μ_B (MPa)	K_B (MPa)
Case S1	8×10^4	6×10^4	4×10^4	6×10^4
Case S2	1×10^4	6×10^4	4×10^4	6×10^4
Series l	$0.025\mu_B \sim 2.25\mu_B$	6×10^4	$2 \times 10^4, 4 \times 10^4$	6×10^4

Checking the microscopic damage of each individual grain, we find that, for both cases, grain damage exists only in the mineral type that has the smaller shear modulus (Figure 5(c)), which is consistent with the experimental observation of granite that intragranular cracks occur in weaker mineral constituents such as feldspar and biotite grains (Eberhardt et al., 1999). As expected, grain damage is more important when the orientation of the plane of weakness (θ) is close to 90^o, i.e. when the orientation of the plane of weakness is close to that of the loading axis (Figure 1). We track two grains belonging to the damaged mineral for further investigation: Grain No. 180 with $\theta = 84^o$ and Grain No. 200 with $\theta = 90^o$. The microscopic damage in these grains (Figure 5(d)) follows an evolution similar to that of the macroscopic matrix damage, with higher values (Figure 5(a)): damage in these two grains reaches values up to 0.2, whereas macroscopic damage remains smaller than 0.02 for the polycrystal. Damage initiation and propagation in each grain depend on the orientation of the grain's plane of weakness and on the grain's mineral type.

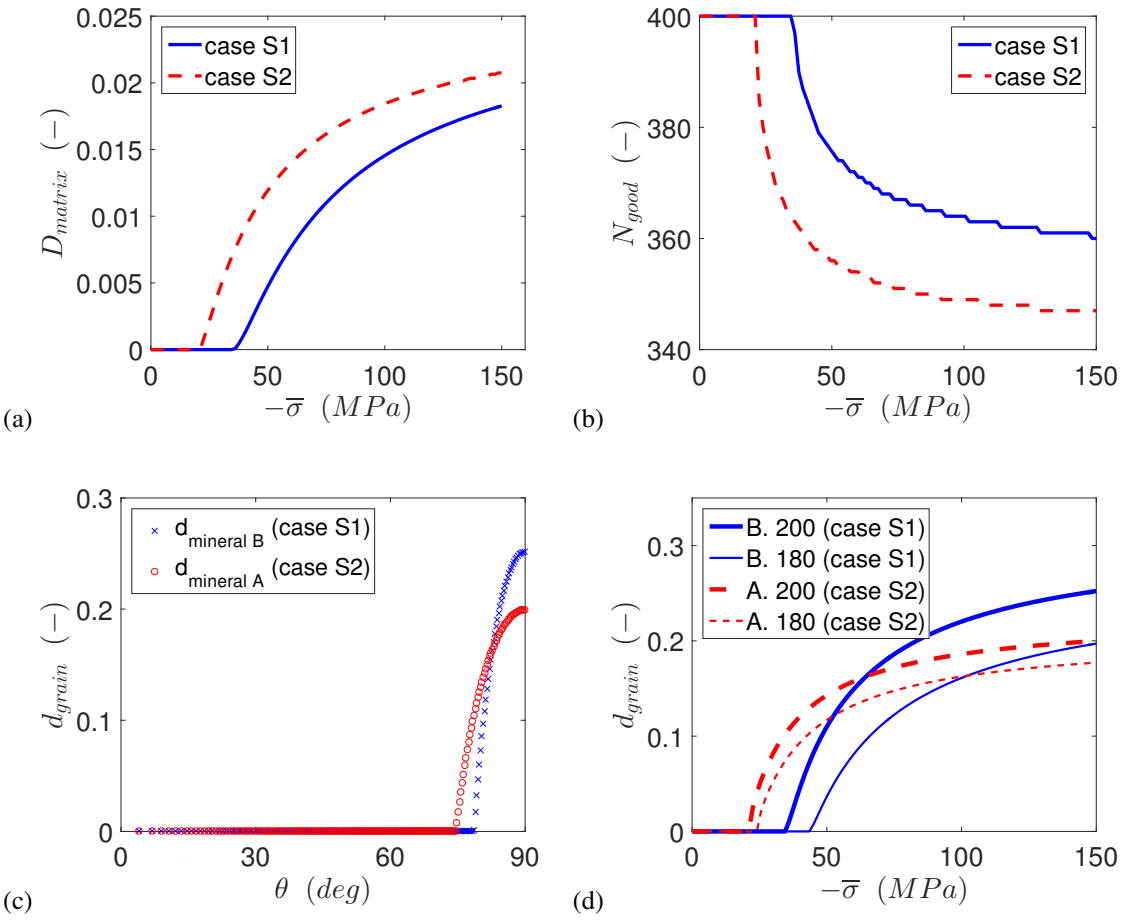

Figure 5. Simulations of uniaxial compression tests with several contrasts in minerals' shear moduli. (a) Matrix damage evolution; (b) Evolution of the number of non-damaged grains; (c) Distribution of microscopic damage; (d) Damage evolutions in grains No. 180 ($\theta = 84^o$) and No. 200 ($\theta = 90^o$).

To further investigate the influence of the contrast in minerals' shear moduli on macroscopic damage, we carry out a series of simulations with μ_A varying between 0.025 μ_B and 2.25 μ_B, with μ_B fixed to two possible values (Table 3). Without any contrast (contrast ratio $\mu_A/\mu_B = 1$), the two types of minerals are mechanically equivalent. In that case, the microscopic stress is equal to the macroscopic stress in all grains, and since the macroscopic stress is compressive, the tensile damage criterion is not reached in the grains. Therefore, the macroscopic damage does not initiate in the matrix (Figure 6). Damage

increases as the contrast ratio departs from unity. However, the increasing trend is asymmetric, i.e. results differ for $\mu_A/\mu_B < 1$ and $\mu_A/\mu_B > 1$. This is due to the fact that the effective shear modulus of the matrix is smaller for the cases studied when $\mu_A/\mu_B < 1$ than for the cases studied when $\mu_A/\mu_B > 1$. By comparing the results for the two different values of μ_B, we find that at equal value of μ_A, the macroscopic damage increases with μ_B, because the shear modulus of the overall matrix increases with μ_B. For the smaller values of μ_A, when the mechanical behavior of mineral A tends to that of a void material, the contribution from mineral B to the overall behavior of the matrix becomes negligible, and the predicted matrix damage is similar in both series of simulations (Figure 6).

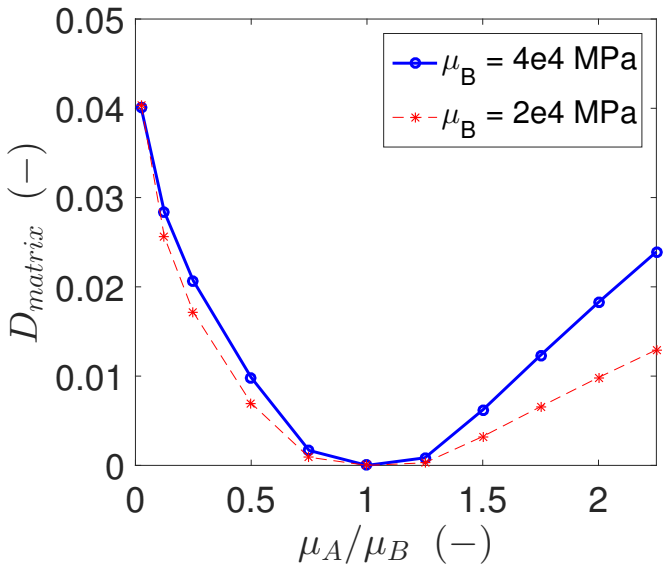

Figure 6. Macroscopic damage in the matrix for different shear modulus contrasts (series *l*).

Influence of Minerals' Bulk Modulus

To examine the influence of the bulk modulus, which measures the compressibility of the matrix and its constituents, we compare two composites made of two mineral constituents of equal shear modulus but distinct bulk moduli, both represented by 200 grains with weakness planes, the orientations of which are uniformly distributed in the [0, $\pi/2$] interval. We study two cases B1 and B2, described in Table 4.

With a contrast in minerals' bulk moduli, the material behaves differently both at the macroscopic and microscopic scales (Figure 7). The Young's modulus of the composite material studied in case B1 is 9 times smaller than that of the composite studied in case B2. Therefore, the stress-strain curve in the

Table 4. Elastic properties of the two minerals used to study the influence of the bulk modulus.

Mineral Type	Mineral A		Mineral B	
Elastic Properties	μ_A (MPa)	K_A (MPa)	μ_B (MPa)	K_B (MPa)
Case B1	4×10^4	6×10^4	4×10^4	2×10^4
Case B2	4×10^4	6×10^4	4×10^4	18×10^4
Series m	4×10^4	$0.375K_B \sim 2K_B$	4×10^4	8×10^4, 16×10^4

loading direction (ε_1) is steeper in case B2 than in case B1 (Figure 7(a)). After reaching the damage threshold, grain damage develops, causing stiffness degradation that manifests by a slope change in the stress-strain curve in the lateral direction (ε_3) (Figure 7(a)). A compressible material tends to be less brittle than a material with high bulk modulus. That is why compared to case B1, an earlier damage initiation and higher damage accumulation is observed in case B2 (Figure 7(b)). Correspondingly at the microscopic scale, we observe an earlier grain damage initiation and a higher number of damaged grains in case B2 (Figure 7(c)). We also note that grain damage develops in one mineral type only, that with the higher Young's modulus (Figure 7(d)). As expected, microscopic damage increases with the angle of orientation of the plane of weakness, i.e. damage accumulates preferentially in grains that have a plane of weakness oriented close the direction of loading, because tensile stresses develop preferentially in the direction perpendicular to the loading axis.

To further investigate the influence of the contrast in minerals' bulk moduli on macroscopic damage, we carry out a series of simulations with K_A varying between 0.375 K_B and 2 K_B, with K_B fixed to two possible values (Table 4). Like in the previous study of the shear modulus, the macroscopic damage does not initiate in the matrix when there is no contrast of mechanical properties between the two minerals, i.e. when $K_A/K_B = 1$ (Figure 8). Damage increases as the contrast ratio departs from unity. Results differ for $K_A/K_B < 1$ and $K_A/K_B > 1$, and suggest that the rate of matrix damage accumulation decreases when the overall bulk modulus of the composite increases. By comparing the results for the two different values of K_B, we find that for the same contrast ratio, the macroscopic damage increases slightly with K_B, because the bulk modulus of the overall matrix is higher, which corresponds to a less compressible and more damageable composite.

Influence of the Mineral Fraction

In the previous parametric studies, we focused on composites with equal mineral fractions for both constituents. However, the volume fraction of the different minerals is unlikely to be uniform in real materials, and the effect of volume fraction of various grains on the material deformation and strength could be significant (Heilbronner and Bruhn, 1998). We study the influence of the minerals' volumetric

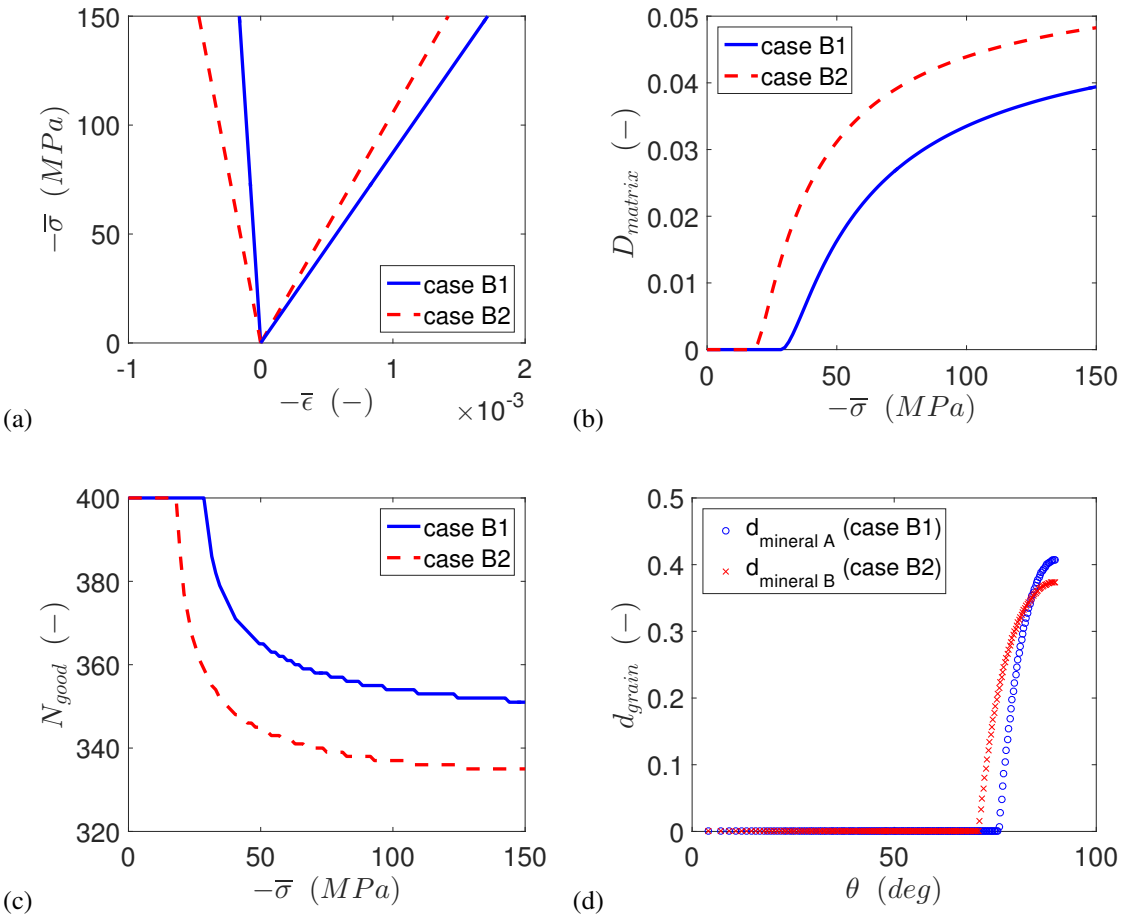

Figure 7. Simulations of uniaxial compression tests with several contrasts in minerals' bulk moduli. (a) Stress-strain relation; (b) Macroscopic damage evolution; (c) Evolution of the number of non-damaged grains; (d) Distribution of microscopic damage.

fraction by varying the number of weakness plane orientations in each mineral type. Three series of tests are conducted, as described in Table 5: contrast in bulk modulus (series i), contrast in shear modulus (series j) and contrast in both shear modulus and bulk modulus (series k). The total number of grains is fixed to 400 and the volumetric fraction of each mineral varies from 5% to 95%, with a 5% interval. Since damage does not initiate in a homogeneous matrix with only one type of mineral, cases with 0% and 100% volumetric ratios are not tested.

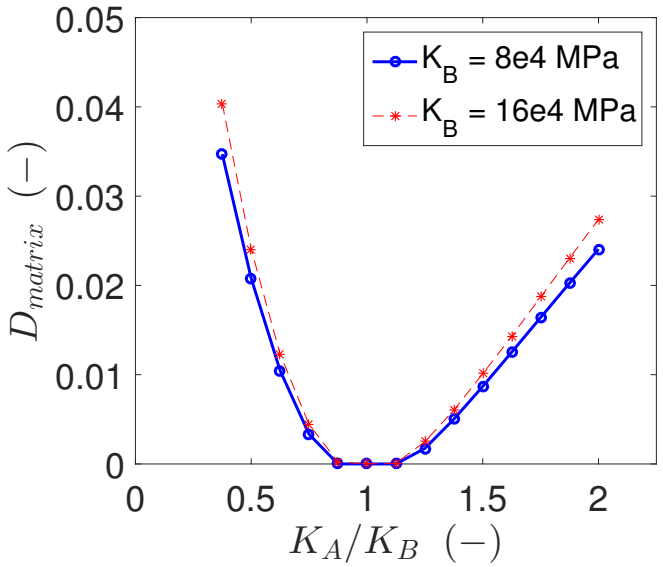

Figure 8. Macroscopic damage in the matrix for different bulk modulus contrasts (series m).

Table 5. Minerals' elastic properties in the study of volumetric fractions and property contrasts $(i, j, k = 1, 2, 3, ..., 19)$.

Mineral Type	Mineral A			Mineral B		
Properties	μ_A (MPa)	K_A (MPa)	N_A	μ_B (MPa)	K_B (MPa)	N_B
Series i	4×10^4	6×10^4	$20 \times i$	4×10^4	18×10^4	$= 400 - N_A$
Series j	1×10^4	6×10^4	$20 \times j$	4×10^4	6×10^4	$= 400 - N_A$
Series k	1×10^4	6×10^4	$20 \times k$	4×10^4	6×10^4	$= 400 - N_A$

Results show that the mineral fraction has a strong influence on matrix damage (Figure 9). Similar parabolic damage variations are observed in the three test series: matrix damage increases first before reaching the peak and then decreases, as the volumetric ratio of mineral type A changes from 5% to 95%. In series i and j, the contrast between elastic properties is relatively small, causing smaller damage in the matrix and a more symmetric damage evolution curve with a peak located between a volume fraction between 45% and 50%. However, with a more significant contrast of elastic properties in series k, heterogenity-induced stress concentrations are more intense and cause a strongly asymmetric response with a peak damage at a mineral fraction of about 75%.

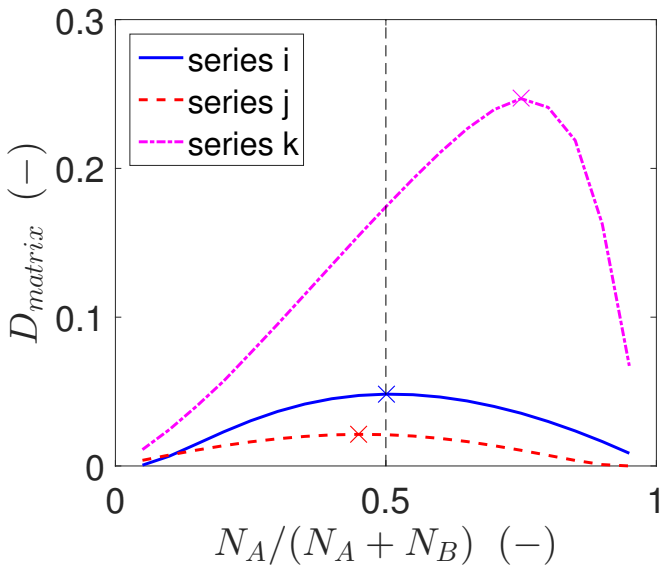

Figure 9. Dependence of matrix damage on the mineral fraction. Crosses indicate peak values.

According to Figures 9 and 10, in series i, the evolution of the macroscopic damage with stress does not follow the symmetry of the curve showing the variations of the matrix damage with the volume fraction of the non-damageable mineral fraction (type A). In other words, the evolution of the matrix damage with stress for $N_A/(N_A+N_B)$ is not the same as that for $1-N_A/(N_A+N_B)$. The same comment applies to the evolution of the number of non-damaged grains with stress. Different mineral compositions that lead to the same ultimate macroscopic damage usually follow very different damage paths (Figure 10(a)). For instance, the macroscopic damage at point P corresponds to $N_A=80$, $N_B=320$ on a blue path, and to $N_A=340$, $N_B=60$ on a green path. Different damage evolution paths are associated to different ultimate numbers of damaged grains: as can be seen in Figure 10(b), we have 70 damaged grains at P_1 ($N_A=80$, $N_B=320$) and 23 damaged grains at P_2 ($N_A=340$, $N_B=60$). According to Figure 10, composites with a lower number of damageable grains tend to start cracking earlier.

Influence of the Orientation Distribution of the Minerals' Planes of Weakness

Each grain contains a plane of weakness, oriented in a pre-assigned direction. In this section, instead of assuming that the orientation angle is uniformly distributed in the interval $[0,\pi/2]$ for both mineral types, we assume that the planes of weakness for one mineral are uniformly distributed in an interval of $\pi/20$ radians, centered about six possible different values (Table 6). The minerals' elastic properties and

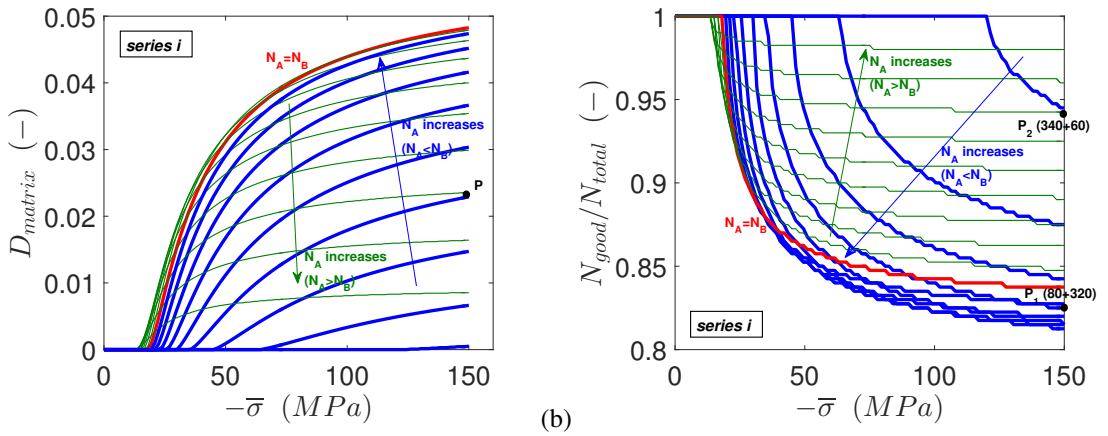

Figure 10. Simulation results of series i with contrasts in bulk modulus at different mineral fractions. (a) Matrix damage evolution; (b) Normalized number of non broken grains.

volumetric fractions are kept the same in the six cases investigated, in order to focus the discussion on the orientation of the weakness planes.

Table 6. Minerals's properties in the study of the orientation of planes of weakness.

Mineral Type	Mineral A				Mineral B			
Properties	μ_A (MPa)	K_A (MPa)	N_A	θ_A (rad)	μ_B (MPa)	K_B (MPa)	N_B	θ_B (rad)
Case D1	4×10^4	6×10^4	200	$0\sim\frac{\pi}{2}$	4×10^4	18×10^4	200	$0\sim\frac{\pi}{20}$
Case D2	4×10^4	6×10^4	200	$0\sim\frac{\pi}{2}$	4×10^4	18×10^4	200	$\frac{9\pi}{40}\sim\frac{11\pi}{40}$
Case D3	4×10^4	6×10^4	200	$0\sim\frac{\pi}{2}$	4×10^4	18×10^4	200	$\frac{9\pi}{20}\sim\frac{\pi}{2}$
Case D4	4×10^4	6×10^4	200	$0\sim\frac{\pi}{20}$	4×10^4	18×10^4	200	$0\sim\frac{\pi}{2}$
Case D5	4×10^4	6×10^4	200	$\frac{9\pi}{40}\sim\frac{11\pi}{40}$	4×10^4	18×10^4	200	$0\sim\frac{\pi}{2}$
Case D6	4×10^4	6×10^4	200	$\frac{9\pi}{20}\sim\frac{\pi}{2}$	4×10^4	18×10^4	200	$0\sim\frac{\pi}{2}$

From the previous sensitivity analysis on the bulk modulus, we know that damage only develops in mineral B, which has a higher bulk modulus. Among all grains belonging to mineral type B, only those with a weakness plane oriented by an angle θ close to $\pi/2$ are prone to damage, because the uniaxial load is applied in direction z (Figure 1). In cases D1 and D2, weakness planes are roughly orthogonal to the loading direction, grains remain undamaged, and no macroscopic damage is produced (Figure 11). By contrast, when weakness planes are close to vertical (θ close to $\pi/2$), damage easily initiates and propagates, which explains why the matrix material representing case D3 shows the highest damage.

Since damage exists in mineral B only, varying the range of θ for mineral type A has no influence on the matrix damage and on the number of non-damaged grains, i.e. cases D4, D5, and D6 provide the same results. Damage obtained in cases D4, D5, and D6 is much smaller than in case D3, because the volumetric fraction of damageable grains with a weakness plane oriented close to the loading direction is higher in case D3.

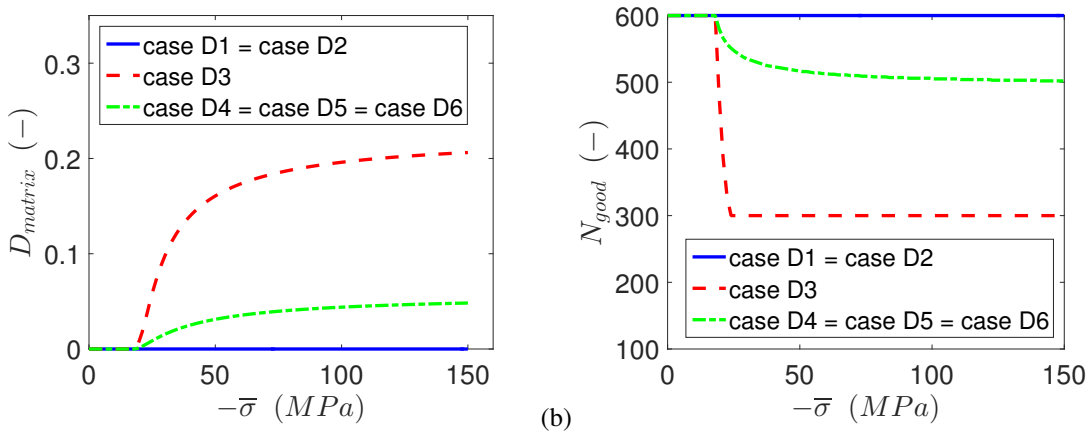

Figure 11. Influence of the orientation distribution of the minerals' planes of weakness. (a) Macroscopic damage evolution; (b) Evolution of the number of non-damaged grains.

Loading-unloading-reloading Stress Paths

To investigate the mechanical behavior of the polycrystal under extreme conditions, we increase the maximum uniaxial compression from 150 MPa to 300 MPa and implement a loading-unloading-reloading stress path. We consider a composite that contains a higher fraction of quasi incompressible minerals that have planes of weakness oriented close to the loading direction (Table 7). The tensile strength σ_T is equal to 6 MPa like in the previous cases. The brittleness indicator η is assumed to be equal to 20, which corresponds to a less brittle polycrystal than in the previous cases.

Table 7. Properties of the material subjected to a uniaxial loading-unloading stress path.

Mineral Type	Mineral A				Mineral B			
Properties	μ_A (MPa)	K_A (MPa)	N_A	θ_A (rad)	μ_B (MPa)	K_B (MPa)	N_B	θ_B (rad)
Value	4×10^4	6×10^4	200	$0 \sim \frac{\pi}{2}$	4×10^4	6×10^6	300	$\frac{9\pi}{20} \sim \frac{\pi}{2}$

The stress-strain curve along the lateral direction follows the expected trend and shows a clear deviation from the linear elastic case indicated by the dashed line (Figure 12(a)). The material behavior is linear-elastic before reaching the damage threshold (O_1O_2). As shown in the magnified image in the lower left corner, the slope of the stress-strain curve decreases after damage initiation during the loading stage (O_2O_3), and remains linear during unloading (O_3O_4). The stress/strain curve obtained during reloading matches that obtained during the unloading until stress reaches the maximum value imposed during the first loading phase. Beyond that point (O_3), the damage threshold is reached, damage propagates again and the slope of the stress/strain curve decreases due to stiffness degradation (O_3O_5). The evolution of the macroscopic damage in the matrix is monotonic except during the elastic unloading stages (Figure 12(b)). The ultimate macroscopic damage variable reaches more than 36%, due to the extreme loading conditions, the high contrast of mineral's bulk moduli and the narrow orientation distribution of weakness planes' orientations in the damageable minerals. For this amount of damage, we observe various decrease in stiffness components, ranging from 0 (C_{3333}) to about 40% (C_{1111}), which highlights the expected anisotropic behavior of the matrix.

At the microscopic scale, we observe that all grains belonging to mineral B are damaged and the damage values reach more than 60% after the first loading and more than 80% after reloading (Figure 12(c)). The values of damage are similar in all grains because all grains have similar θ values. All the grains belonging to mineral A remain undamaged, even for the grains that have a plane of weakness oriented by an angle close to 90 degrees to the horizontal. This observation is consistent with the previous results obtained, because grains of mineral B have larger bulk modulus than those of mineral A. Grains start to break soon after the load is applied. The number of damaged grains reaches a maximum at a relatively moderate load (Figure 12(d)). Upon reloading, no more grains get damaged, but damage in the grains that were already damaged during the first loading stage increases.

Conclusions

In this work, an inclusion-matrix model is proposed to understand the micromechanical processes that trigger the initiation and propagation of damage in heterogeneous polycrystalline materials. The inclusion-matrix interaction law is a key element of the formulation because of the numerous complexities of the matrix behavior. This study focuses on the damage accommodation of the matrix, i.e., on the effect of the matrix damaging process on the interaction law between the inclusion and the matrix. The challenge is that the inclusion-matrix interaction law depends on the matrix stiffness which itself depends on the macroscopic damage, a priori unknown. The main research contribution presented in this paper is the incremental method that is used to solve the system of implicit equations at the foundation of the inclusion-matrix model. The propagation of cracks along planes of weakness of

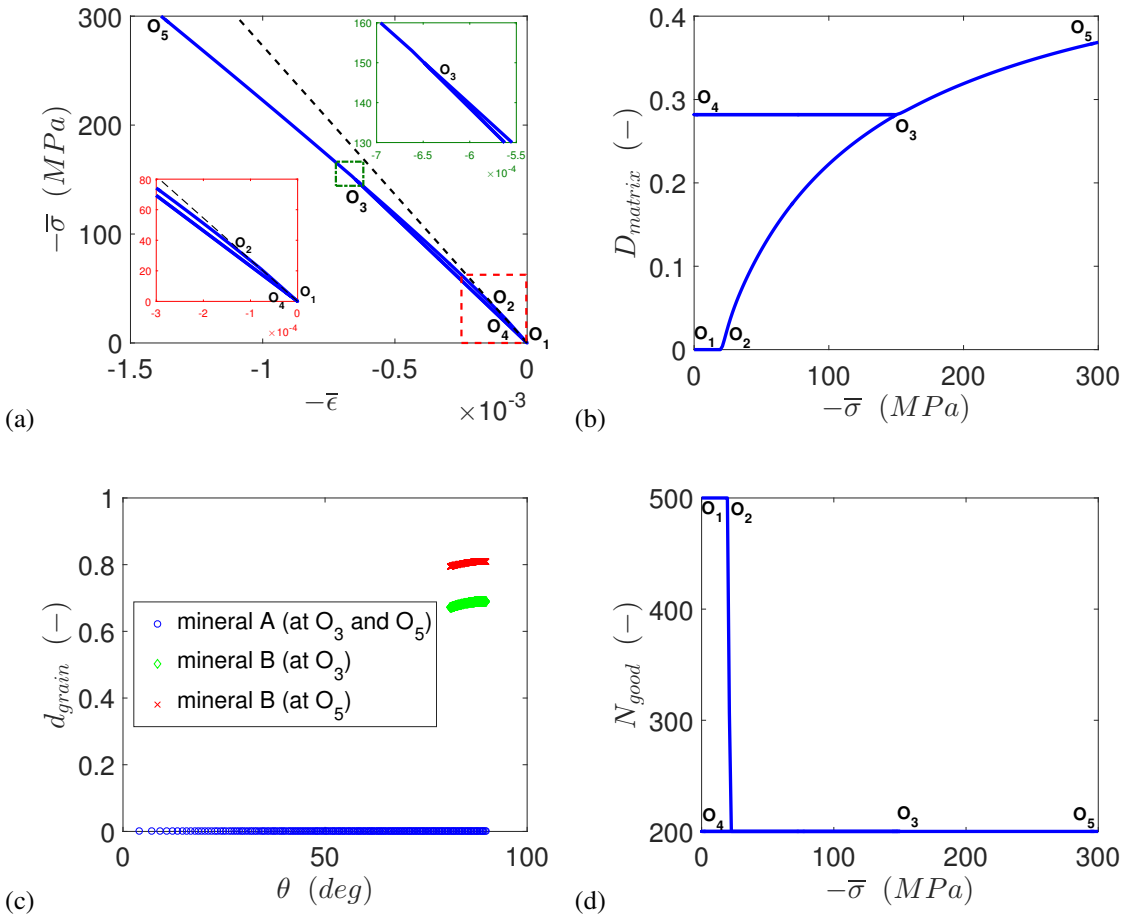

Figure 12. Macro- and micro- behavior of the material subjected to a loading-unloading-reloading path. (a) Stress-strain relation; (b) Macroscopic damage evolution; (c) Distribution of microscopic damage; (d) Evolution of the number of non-damaged grains.

various orientation distributions results in mechanical anisotropy in the matrix. Another originality of the proposed inclusion-matrix interaction model is the account for the anisotropy of the matrix. It is assumed that the matrix follows an ellipsoidal anisotropic behavior. A summary of the equations involved in the explicit expression of the Hill's tensor for a matrix that has an ellipsoidal type of anisotropy is provided in the appendix; more details will be published in a paper in preparation.

Damage in minerals is assumed to result from the propagation of cracks along weakness planes that are present in the crystalline structure. In order to focus on the mathematical and numerical aspects of the resolution method for the micromechanical model, only one weakness plane was considered for each mineral. The orientation of the weakness plane relative to the loading axis was assigned a variable probability density function in the parametric studies presented. A softening damage model was used to represent the cracking process at the mineral scale.

A composite made of two types of mineral inclusions is used as an example throughout this study. The model is calibrated against experimental data available for granite. Although the physical meaning of the results obtained in the simulations needs to be confirmed by additional experimental and numerical cases, we can draw the following main conclusions. In the context of a simple uniaxial compression load applied to the polycrystal, the damage always occurred in only one type of mineral, due to contrasts of micromechanical properties: the damaging mineral was that with a smaller shear modulus (respectively higher bulk modulus) when the bulk modulus (respectively shear modulus) was the same. For two minerals with the same shear modulus but different bulk moduli, the maximum damage in the polycrystal under a given load was obtained when the volume fraction of the two minerals was the same. For two minerals with different shear moduli, the macroscopic damage was not always maximum at equal mineral fractions. Another interesting result was that when the orientation of the weakness planes in the damaging mineral laid within a narrow interval close to the orientation of the loading axis, the macroscopic damage behavior was more brittle than when the orientations were distributed over a wider interval.

This paper provides the foundation of a micromechanical model for quasi-brittle materials taking into account the elastic-damage accommodation of the matrix and presents an original method to solve the system of implicit equations involved in the formulation. Parametric studies show that upon proper calibration, the proposed model can be extended to understand and predict the micro-macro behavior of brittle materials such as concrete, ceramics and hard rocks. Future work will focus on the micromechanical modeling of the coupling between the visco-plastic and damage accommodation of the matrix. An infinite number of planes of weakness will also be considered to allow extending the present formulation with spherical inclusions to both intra- and inter-granular damage.

Declaration of conflicting interests

The author(s) declared no potential conflicts of interest with respect to the research, authorship, and/or publication of this article.

Funding

The author(s) disclosed receipt of the following financial support for the research, authorship, and/or publication of this article: U.S. Nationsal Science Foundation grant CMMI 1362004/1361996.

References

Abdul-Latif A and Mounounga T (2009) Damage-induced anisotropy with damage deactivation. *International Journal of Damage Mechanics* 18(2): 177–198.

Berveiller M and Zaoui A (1978) An extension of the self-consistent scheme to plastically-flowing polycrystals. *Journal of the Mechanics and Physics of Solids* 26(5): 325–344.

Boudifa M, Saanouni K and Chaboche JL (2009) A micromechanical model for inelastic ductile damage prediction in polycrystalline metals for metal forming. *International Journal of Mechanical Sciences* 51(6): 453 – 464.

Brown JM, Angel RJ and Ross NL (2016) Elasticity of plagioclase feldspars. *Journal of Geophysical Research: Solid Earth* 121(2): 663–675. 2015JB012736.

Buchheit TE, Wellman GW and Battaile CC (2005) Investigating the limits of polycrystal plasticity modeling. *International Journal of Plasticity* 21(2): 221–249.

Budiansky B and O'connell RJ (1976) Elastic moduli of a cracked solid. *International Journal of Solids and Structures* 12(2): 81 – 97.

Chaboche JL (1992) Damage induced anisotropy: On the difficulties associated with the active/passive unilateral condition. *International Journal of Damage Mechanics* 1(2): 148–171.

Chaboche JL, Kruch S, Maire J and Pottier T (2001) Towards a micromechanics based inelastic and damage modeling of composites. *International Journal of Plasticity* 17(4): 411–439.

Cleary M, Lee S and Chen I (1980) Self-consistent techniques for heterogeneous media. *Journal of the Engineering Mechanics Division* 106(5): 861–887.

Daley P and Hron F (1979) Reflection and transmission coefficients for seismic waves in ellpsoidally anisotropic media. *Geophysics* 44(1): 27–38.

Dragon A, Halm D and Dsoyer T (2000) Anisotropic damage in quasi-brittle solids: modelling, computational issues and applications. *Computer Methods in Applied Mechanics and Engineering* 183(34): 331–352.

Eberhardt E, Stimpson B and Stead D (1999) Effects of grain size on the initiation and propagation thresholds of stress-induced brittle fractures. *Rock Mechanics and Rock Engineering* 32(2): 81–99.

Eshelby JD (1957) The determination of the elastic field of an ellipsoidal inclusion, and related problems. *Proceedings of the Royal Society of London A: Mathematical, Physical and Engineering Sciences* 241(1226): 376–396.

Feng XQ and Yu SW (2010) Damage micromechanics for constitutive relations and failure of microcracked quasi-brittle materials. *International Journal of Damage Mechanics* 19(8): 911–948.

Halm D and Dragon A (1988) An anisotropic model of damage and frictional sliding for brittle materials. *Eur. J. Mech. A/Solids* 17(3): 439–460.

Halm D and Dragon A (2002) Modelisation de l'endommagement par mesofissuration du granite. *Revue Francaise de Genie Civil* 6(1): 21–33.

Heilbronner R and Bruhn D (1998) The influence of three-dimensional grain size distributions on the rheology of polyphase rocks. *Journal of Structural Geology* 20(6): 695–705.

Hershey A (1954) The elasticity of an isotropic aggregate of anisotropic cubic crystals. *Journal of Applied Mechanics* 21: 236–240.

Heyliger P, Ledbetter H and Kim S (2003) Elastic constants of natural quartz. *The Journal of the Acoustical Society of America* 114(2): 644–650.

Hill R (1952) The elastic behaviour of a cryscrystal aggregate. *Proceedings of the Physical Society. Section A* 65(5): 349–354.

Hill R (1965a) Continuum micro-mechanics of elastoplastic polycrystals. *Journal of the Mechanics and Physics of Solids* 13(2): 89–101.

Hill R (1965b) A self-consistent mechanics of composite materials. *Journal of the Mechanics and Physics of Solids* 13(4): 213–222.

Horii H and Nemat-Nasser S (1983) Overall moduli of solids with microcracks: Load-induced anisotropy. *Journal of the Mechanics and Physics of Solids* 31(2): 155–171.

Horii H and Nemat-Nasser S (1985) Compression-induced microcrack growth in brittle solids: Axial splitting and shear failure. *Journal of Geophysical Research* 90(B4): 3105–3125.

Ju JW (1991) On two-dimensinal self-consistent micromechanical damage models for brittle solids. *International Journal of Solids and Structures* 27(2): 227 – 258.

Ju JW (1996) On micromechanical evolutionary damage models for polycrystalline ceramics. *International Journal of Damage Mechanics* 5(2): 113–137.

Kachanov M (1980) Continuum model of medium with cracks. *Journal of Engineering Mechanics Division, ASCE* 106(5): 1039–1051.

Kachanov M (1992) Effective elastic properties of cracked solids: critical review of some basic concepts. *Applied Mechanics Reviews* 45(8): 304–355.

Kneer G (1965) ber die berechnung der elastizittsmoduln vielkristalliner aggregate mit textur. *physica status solidi (b)* 9(3): 825–838.

Kröner E (1961) Zur plastischen verformung des vielkristalls. *Acta metallurgica* 9(2): 155–161.

Lee X and Ju JW (1991) Micromechanical damage models for brittle solids. part ii: compressive loadings. *Journal of Engineering Mechanics* 117(7): 1515–1536.

Lekhnitskii S (1963) *Theory of Elasticity of An Anisotropic Elastic Body*. San Francisco: Holden Day Series in Mathematical Physics.

Louis L, Robion P and David C (2004) A single method for the inversion of anisotropic data sets with application to structural studies. *Journal of Structural Geology* 26(11): 2065 – 2072.

Masson R, Bornert M, Suquet P and Zaoui A (2000) An affine formulation for the prediction of the effective properties of nonlinear composites and polycrystals. *Journal of the Mechanics and Physics of Solids* 48(67): 1203–1227.

Masson R and Zaoui A (1999) Self-consistent estimates for the rate-dependentelastoplastic behaviour of polycrystalline materials. *Journal of the Mechanics and Physics of Solids* 47(7): 1543–1568.

Mercier S and Molinari A (2009) Homogenization of elastic–viscoplastic heterogeneous materials: Self-consistent and mori-tanaka schemes. *International Journal of Plasticity* 25(6): 1024–1048.

Milgrom M and Shtrikman S (1992) The energy of inclusions in linear media exact shape-independent relations. *Journal of the Mechanics and Physics of Solids* 40(5): 927 – 937.

Milton G (2002) *The Theory of Composites*. Cambridge University Press.

Molinari A, Ahzi S and Kouddane R (1997) On the self-consistent modeling of elastic-plastic behavior of polycrystals. *Mechanics of Materials* 26(1): 43–62.

Molinari A, Canova G and Ahzi S (1987) A self consistent approach of the large deformation polycrystal viscoplasticity. *Acta Metallurgica* 35(12): 2983–2994.

Nemat-Nasser S (2004) *Plasticity: a treatise on finite deformation of heterogeneous inelastic materials*. Cambridge University Press.

Nemat-Nasser S and Hori M (2013) *Micromechanics: overall properties of heterogeneous materials*. Elsevier.

Nemat-Nasser S and Obata M (1988) A microcrack model of dilatancy in brittle materials. *Journal of Applied Mechanics* 55(1): 24–35.

Paliwal B and Ramesh K (2008) An interacting micro-crack damage model for failure of brittle materials under compression. *Journal of the Mechanics and Physics of Solids* 56(3): 896 – 923.

Perras MA and Diederichs MS (2014) A review of the tensile strength of rock: Concepts and testing. *Geotechnical and Geological Engineering* 32: 525–546.

Pouya A (2007) Ellipsoidal anisotropies in linear elasticity - extension of saint venant's work to phenomenological modelling of materials. *International Journal of Damage Mechanics* 16: 95–126.

Pouya A (2011) Ellipsoidal anisotropy in linear elasticity: Approximation models and analytical solutions. *International Journal of Solids and Structures* 48(1415): 2245–2254.

Pouya A and Zaoui A (1999) Linearisation and homogenization for viscoelastic materials. *Comptes-Rendus de I'Academie des Sciences de Paris* 327(II b): 365–370.

Pouya A and Zaoui A (2006) A transformation of elastic boundary value problems with application to anisotropic behavior. *International Journal of Solids and Structures* 43(16): 4937–4956.

Pouya A, Zhu C and Arson C (2016) Micro-macro approach of salt viscous fatigue under cyclic loading. *Mechanics of Materials* 93: 13–31.

Qi M, Giraud A, Colliat JB and Shao JF (2016) A numerical damage model for initially anisotropic materials. *International Journal of Solids and Structures* 100: 245–256.

Reuss A (1929) Berechnung der fliepgrenze von mischkristallen auf grund der plastizitatsbedingung fur einkristalle. *Zeitschrift fr Angewandte Mathematik und Mechanik* 9: 49–58.

Rougier Y, Stolz C and Zaoui A (1994) Self-consistent modelling of elastic-viscoplastic polycrystals. *C.R. Acad. Sci. Paris, série II* 318(2): 145–151.

Saint Venant B (1863) Sur la distribution des lasticits autour de chaque point dun solide ou dun milieu de contexture quelconque, particulirement lorsquil est amorphe sans łtre isotrope. *Journal de Math. Pures et Appliquees, Tome VIII* 2: 257–430.

Sevostianov I and Kachanov M (2002) Explicit cross-property correlations for anisotropic two-phase composite materials. *Journal of the Mechanics and Physics of Solids* 50(2): 253–282.

Sevostianov I and Kachanov M (2008) On approximate symmetries of the elastic properties and elliptic orthotropy. *International Journal of Engineering Science* 46(3): 211–223.

Sumarac D and Krajcinovic D (1987) A self-consistent model for microcrack-weakened solids. *Mechanics of Materials* 6(1): 39 – 52.

Voigt W (1910) *Lehrbuch der Kristallphysik*. Leipzig.

Wang W, Shao J, Zhu Q and Xu W (2015) A discrete viscoplastic damage model for time-dependent behaviour of quasi-brittle rocks. *International Journal of Damage Mechanics* 24(1): 21–40.

Weng G (1982) A unified self-consistent theory for the plastic-creep deformation of metals. *J. Appl. Mech* 49: 728–734.

Willis J (1977) Bounds and self-consistent estimates for the overall properties of anisotropic composites. *Journal of the Mechanics and Physics of Solids* 25(3): 185–202.

Wu P, Neale K and Van der Giessen E (1996) Simulation of the behaviour of fcc polycrystals during reversed torsion. *International Journal of Plasticity* 12(9): 1199–1219.

Zeng T, Shao JF and Xu W (2014) Modeling of viscoplastic deformation in geomaterials with a polycrystalline approach. *International Journal of Rock Mechanics and Mining Sciences* 72: 182–190.

Zeng T, Shao JF and Xu W (2015) A micromechanical model for the elastic–plastic behavior of porous rocks. *Computers and Geotechnics* 70: 130–137.

Zhu C, Pouya A and Arson C (2016) Prediction of viscous cracking and cyclic fatigue of salt polycrystals using a joint-enriched finite element model. *Mechanics of Materials* 103: 28 – 43.

Zhu QZ, Kondo D and Shao J (2008) Micromechanical analysis of coupling between anisotropic damage and friction in quasi brittle materials: role of the homogenization scheme. *International Journal of Solids and Structures* 45(5): 1385–1405.

Zhu QZ and Shao JF (2015) A refined micromechanical damage–friction model with strength prediction for rock-like materials under compression. *International Journal of Solids and Structures* 60: 75–83.

Appendix 1: Hill's Stiffness Tensor for a Matrix with Ellipsoidal Anisotropy

Consider a matrix with the elastic tensor:

$$C_{ijkl}(\boldsymbol{D}) \;=\; \lambda\, D_{ij} D_{kl} \;+ \mu\,(D_{ik} D_{jl} \;+ D_{il} D_{jk}) \tag{33}$$

with $\boldsymbol{D}$ having axial symmetry around the axis $\underline{N}$:

$$\boldsymbol{D} = cos^2\omega\;\boldsymbol{\delta} + sin^2\omega \underline{N} \;\otimes \underline{N} \tag{34}$$

By taking the x_3-axis parallel to $\underline{N}$, and noting $cos^2\omega = \sqrt{1-D}$, we obtain:

$$\boldsymbol{D} = \begin{bmatrix} \sqrt{1-D} & & \\ & \sqrt{1-D} & \\ & & 1 \end{bmatrix} \tag{35}$$

The Hill's stiffness tensor $\boldsymbol{L^*}$ for a spherical cavity in an infinite matrix is related to the polarization tensor $\boldsymbol{\Lambda}$ by Kneer (1965):

$$\Lambda_{ijkl} = (L^* + C)^{-1}_{ijkl} \tag{36}$$

For the above ellipsoidal stiffness tensor $\boldsymbol{C}$, the polarization tensor is given by the following relations:

$$\Lambda_{ijkl} = \frac{1}{4\mu}\left[(\boldsymbol{D}^{-1})_{ik} V_{jl} + (\boldsymbol{D}^{-1})_{il} V_{jk} + (\boldsymbol{D}^{-1})_{jk} V_{il} + (\boldsymbol{D}^{-1})_{jl} V_{ik}\right] - \frac{1}{2\mu(1-\nu)} W_{ijkl} \tag{37}$$

The second and fourth order tensors $\boldsymbol{V}$ and $\boldsymbol{W}$ have axial symmetry about the $\underline{N}$ direction. When the axis x_3 is parallel to $\underline{N}$, the tensor $\boldsymbol{V}$ is diagonal, and the eigenvalues are:

$$V_{11} = V_{22} = \frac{1}{2sin^2\omega}\left(-1 + \frac{\omega}{sin\omega cos\omega}\right), \qquad V_{33} = \frac{1}{sin^2\omega}\left(1 - \omega\frac{cos\omega}{sin\omega}\right) \tag{38}$$

Moreover, the only non-zero components of tensor $\boldsymbol{W}$ are:

$$W_{1111} = W_{2222}, \quad W_{3333}, \quad W_{1122} = W_{1212}, \quad W_{1133} = W_{2233} = W_{1313} = W_{2323} \tag{39}$$

Given by:

$$W_{1111} = \frac{3}{8sin^4\omega}\left[1 + \frac{1}{2cos^2\omega} + \frac{\omega}{sin\omega cos\omega}\left(-2 + \frac{1}{2cos^2\omega}\right)\right] \tag{40}$$

$$W_{3333} = \frac{1}{sin^4\omega}\left(1 + \frac{cos^2\omega}{2} - \frac{3\omega}{2}\frac{cos\omega}{sin\omega}\right) \tag{41}$$

$$W_{1122} = W_{1212} = \frac{1}{3}W_{1111} \tag{42}$$

$$W_{1133} = W_{1313} = \frac{1}{4sin^4\omega}\left[-3 + \frac{\omega}{sin\omega cos\omega}\left(1 + 2cos^2\omega\right)\right] \tag{43}$$

Appendix 2: Damaged Stiffness Tensor of A Grain

In order to ensure that $\widetilde{\boldsymbol{C}}$ possesses ellipsoidal anisotropy with three parameters (see equations (42) and (43) in (Pouya, 2011)), we choose:

$$M_{ijkl}(\boldsymbol{d^{(n)}}) = \frac{1}{2}\left[H^{(n)}_{ik}\,H^{(n)}_{lj} + H^{(n)}_{il}\,H^{(n)}_{kj}\right], \qquad \boldsymbol{H^{(n)}} = \left(\boldsymbol{\delta} - \boldsymbol{d^{(n)}}\right)^{-1/2} \tag{44}$$

where $\boldsymbol{\delta}$ is the second-order identity tensor. The goal of the following derivations is to express explicitly the components of the damaged stiffness tensor $\widetilde{\boldsymbol{C}}$ for the unidirectional damage $\boldsymbol{d^{(n)}} = d^{(n)}\,\boldsymbol{n^{(n)}} \otimes \boldsymbol{n^{(n)}}$.

We define:

$$\boldsymbol{P^{(n)}} = \boldsymbol{H^{(n)}}^{-1} = \left(\boldsymbol{\delta} - \boldsymbol{d^{(n)}}\right)^{+1/2} \tag{45}$$

$$\boldsymbol{Q^{(n)}} = \boldsymbol{P^{(n)}} \cdot \boldsymbol{P^{(n)}} = \boldsymbol{\delta} - d^{(n)}\,\boldsymbol{n^{(n)}} \otimes \boldsymbol{n^{(n)}} \tag{46}$$

The form of the tensor $\boldsymbol{Q^{(n)}}$ imposes the following form for the tensor $\boldsymbol{P^{(n)}}$:

$$\boldsymbol{P^{(n)}} = \boldsymbol{\delta} + \beta \boldsymbol{n^{(n)}} \otimes \boldsymbol{n^{(n)}} \tag{47}$$

where β is a scalar. Since $n_k^{(n)}\, n_k^{(n)} = 1$, we have:

$$Q_{ij}^{(n)} = P_{ik}^{(n)} P_{kj}^{(n)} = \delta_{ij} + 2\beta\, n_i^{(n)}\, n_j^{(n)} + \beta^2\, n_i^{(n)}\, n_j^{(n)} \tag{48}$$

By identification, we get:

$$\beta = -1 + \sqrt{1 - d^{(n)}} \tag{49}$$

We note that $\boldsymbol{H^{(n)}}$ satisfies:

$$\boldsymbol{P^{(n)}} \cdot \boldsymbol{H^{(n)}} = \boldsymbol{H^{(n)}} \cdot \boldsymbol{P^{(n)}} = \boldsymbol{\delta} \tag{50}$$

Therefore, $\boldsymbol{H^{(n)}}$ is of the form:

$$\boldsymbol{H^{(n)}} = \boldsymbol{\delta} + \beta' \boldsymbol{n^{(n)}} \otimes \boldsymbol{n^{(n)}} \tag{51}$$

By identification between equations (50) and (51):

$$\beta' = \frac{d^{(n)} - 1 + \sqrt{1 - d^{(n)}}}{1 - d^{(n)}} \tag{52}$$

Therefore:

$$J_{ijkl}^{(n)} = H_{ik}^{(n)} H_{jl}^{(n)} = \delta_{ik}\delta_{jl} + \beta' \left(\delta_{ik} n_j^{(n)} n_l^{(n)} + \delta_{jl} n_i^{(n)} n_k^{(n)} \right) + (\beta')^2\, n_i^{(n)} n_j^{(n)} n_k^{(n)} n_l^{(n)} \tag{53}$$

From equation 44, we have:

$$M_{ijkl}(d^{(n)}) = \frac{1}{2} \left(J_{ijkl}^{(n)} + J_{ijlk}^{(n)} \right) = I_{ijkl} + \frac{\beta'}{2} \Omega_{ijkl}^{(n)} + (\beta')^2\, \nu_{ijkl}^{(n)} \tag{54}$$

In which we note:

$$\begin{aligned} I_{ijkl} &= \tfrac{1}{2} \left(\delta_{ik}\delta_{jl} + \delta_{il}\delta_{jk} \right) \\ \Omega_{ijkl}^{(n)} &= \delta_{ik} n_j^{(n)} n_l^{(n)} + \delta_{il} n_j^{(n)} n_k^{(n)} + \delta_{jk} n_i^{(n)} n_l^{(n)} + \delta_{jl} n_i^{(n)} n_k^{(n)} \\ \nu_{ijkl}^{(n)} &= n_i^{(n)} n_j^{(n)} n_k^{(n)} n_l^{(n)} \end{aligned} \tag{55}$$

We can show that:

$$\boldsymbol{\Omega^{(n)}} : \boldsymbol{\Omega^{(n)}} \;=\; 2\,\boldsymbol{\Omega^{(n)}} \;+\; 8\,\boldsymbol{\nu^{(n)}} \tag{56}$$

$$\boldsymbol{\Omega^{(n)}} : \boldsymbol{\nu^{(n)}} \;=\; \boldsymbol{\nu^{(n)}} : \boldsymbol{\Omega^{(n)}} \;=\; 4\,\boldsymbol{\nu^{(n)}} \tag{57}$$

$$\boldsymbol{\nu^{(n)}} : \boldsymbol{\nu^{(n)}} \;=\; \boldsymbol{\nu^{(n)}} \tag{58}$$

We note:

$$\boldsymbol{N}(d^{(n)}) \;=\; \boldsymbol{M}^{-1}(d^{(n)}) \tag{59}$$

From equation (54), $\boldsymbol{N}(d^{(n)})$ is of the form:

$$\boldsymbol{N}(d^{(n)}) \;=\; \boldsymbol{I} \;+ b\,\boldsymbol{\Omega^{(n)}} \;+ c\,\boldsymbol{\nu^{(n)}} \tag{60}$$

where b and c are scalars, which are determined by identification:

$$\begin{cases} b \;=\; -\frac{\beta'}{2(1+\beta')} \\ c \;=\; \frac{(\beta')^2}{(1+\beta')^2} \end{cases} \tag{61}$$

The transpose of $\boldsymbol{N}(d^{(n)})$ can now be expressed as follows:

$$(N^T)_{ijkl}(d^{(n)}) \;=\; \delta_{ip}\delta_{jq}N_{qpkl}(d^{(n)}) \;=\; N_{jikl}(d^{(n)}) \tag{62}$$

Since $I_{ijkl} = I_{jikl}$, $\Omega^{(n)}_{ijkl} = \Omega^{(n)}_{jikl}$, $\nu^{(n)}_{ijkl} = \nu^{(n)}_{jikl}$, we have:

$$(N^T)_{ijkl}(d^{(n)}) \;=\; N_{ijkl}(d^{(n)}) \tag{63}$$

Noting λ_0 and μ_0 the initial coefficients of Lamé, the expression of the damaged stiffness tensor is as follows:

$$\begin{aligned}\widetilde{\boldsymbol{C}}(\boldsymbol{d^{(n)}}) \;=\; \lambda_0\,\boldsymbol{\delta}\otimes\boldsymbol{\delta} \;+ 2\mu_0\,\boldsymbol{I} \;+ 4\mu_0 b(1+b)\,\boldsymbol{\Omega^{(n)}} \;+ \left[\lambda_0(4b+c)^2 + 2\mu_0(8b^2+c^2+8bc+2c)\right]\,\boldsymbol{\nu^{(n)}} \\ +\lambda_0(4b+c)\left[\boldsymbol{\delta}\otimes(\boldsymbol{n^{(n)}}\otimes\boldsymbol{n^{(n)}}) + (\boldsymbol{n^{(n)}}\otimes\boldsymbol{n^{(n)}})\otimes\boldsymbol{\delta}\right]\end{aligned} \tag{64}$$

We note that:

$$\beta = -sin^2\alpha_n, \quad \beta' = tan^2\alpha_n, \quad b = -\frac{1}{2}sin^2\alpha_n, \quad c = sin^4\alpha_n \tag{65}$$

Where:

$$cos^2\alpha_n \;=\; \sqrt{1-d^{(n)}} \tag{66}$$

Rewriting equation (64) leads to the following expression for the damaged stiffness tensor of the grain:

$$\begin{aligned}\widetilde{\boldsymbol{C}}(\boldsymbol{d^{(n)}}) \;=\; & \lambda_0\,\boldsymbol{\delta}\otimes\boldsymbol{\delta} \;+ 2\mu_0\,\boldsymbol{I} \;- d^{(n)}\mu_0\,\boldsymbol{\Omega^{(n)}} \;+ \left(d^{(n)}\right)^2(\lambda_0+2\mu_0)\,\boldsymbol{\nu^{(n)}} \\ & -d^{(n)}\lambda_0\left[\boldsymbol{\delta}\otimes(\boldsymbol{n^{(n)}}\otimes\boldsymbol{n^{(n)}}) + (\boldsymbol{n^{(n)}}\otimes\boldsymbol{n^{(n)}})\otimes\boldsymbol{\delta}\right]\end{aligned} \tag{67}$$